Reply to comments, Referee #1

We would like to thank Referee #1 for his/her time, constructive and helpful comments and suggestions. Note, throughout the document R1 stands for reviewer 1, and figures named R1.x point to the x'th figure in "Reply to comments, Referee #1.

General comments:

1. **Since the mean number of degrees of freedom of the NH3 retrieval for both instruments seems to be near 1, comparison of the total NH3-column amounts is a central part of the paper. However, some major retrieval characteristics should additionally be provided. Especially a kind of total column operator, like the one shown by Rodgers and Conner, 2003, Fig. 11. E.g. Fig 5 of the actual draft could be modified such that the AK for absolute concentrations or partial column amounts is provided.**

We agree it would be a good idea to show total column averaging kernels, but with this version of the CrIS retrieval we did not save the required temperature and water vapour input profiles in the output retrieval files to compute accurate total column averaging kernels. In a future version of the retrieval output files we will compute and provide the total column averaging kernels to go along with the total column values. In the case of the FTIR retrievals, the partial column averaging kernel is provided in the datasets. Figure R1.1 shows the partial column averaging kernel for the example as shown in Figure 5.

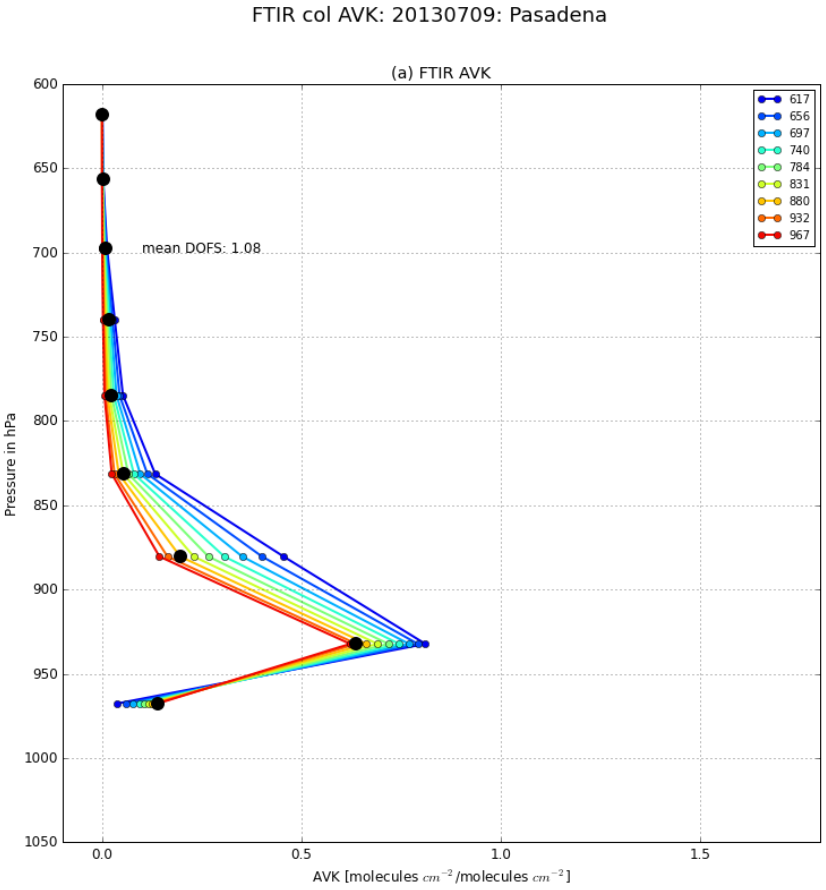

Fig R1.1. FTIR averaging kernel in [molecules cm^{-2} / molecules cm^{-2}]. The black dots show the matrices diagonal values.

2. **Further, in Fig. 5 I wonder why the FTIR AK does not peak at the ground level: is there some problem with half-levels there? This should be explained in the paper.**

The FTIR averaging kernel does not seem to always have complete sensitivity for the ammonia near the surface and varies from observation to observation. As mentioned in the text it usually peaks in between the surface and 850hPa. The method seems to be slightly more sensitive for the second layer in the retrieval. Furthermore, one should take into account that we only have a total DOF of 1 for most observations. Hence one cannot expect a perfect AVK peaking at its own level. We point the referee to the Figures R2.1-R2.4 in our reply to Referee #2.

3. **Also, while error estimations of the profile retrievals are presented, it would be helpful to have those numbers for the total column amounts as well.**

The estimated errors on the FTIR total column amounts are mentioned in section 2.2, being in the order of 30% for which we point you onward to Dammers et al., (2015). In case of CrIS we do not mention a specific percentage in the text, but most total columns have an estimated error in the order of 10 %. This estimate however is on the low side as it does not yet include an estimate for the systematic errors in the retrieval.

Specific comments:

4. **L27-35: The abstract should be made more concise. These lines, which include mainly motivation could be skipped.**

We removed Line 27-35, and edited the abstract to be more concise. Furthermore we made the following edits:
Line 44: Added "(<1.0x1016 molecules cm-2)"
Line 45: Removed "and the FTIR total columns are smaller than 1.0x1016 molecules cm-2,"
Line 46: Removed "are small with CrIS showing"
Line 47: Added "show"
Line 47: Removed "around +2.4 x 1015 (standard deviation = ±5.5 x 1015) molecules cm-2, which corresponds to a relative difference of ~+50% (std = ±100 %)."
Line 48: Added "The CrIS and FTIR profile comparisons differences are mostly within the range of the estimated retrieval uncertainties single level retrieved profile values showing average difference in the range of ~20 to 40%"
Line 50: Removed "for these comparisons"
Line 51: Added "into the boundary layer that typically peaks at"
Line 51: Removed "to"
Line 52: Added "(~1.5 km)"
Line 52: Removed "and"
Line 52: Removed "retrieved profiles also compare well with the"
Line 53: Added "is"
Line 53: Removed "of"
Line 53: Added "std ="
Line 53 Added ","
Line 53 Removed "and a"
Line 53: Added "%"
Line 53: Added "std ="
Line 54: Removed "Most of the absolute and relative profile comparison differences are in the range of the estimated retrieval uncertainties. However, t"
Line 56: Added "At the surface, where CrIS typically has lower sensitivity,"
Line 55: Removed "he CrIS retrieval does"
Line 55: Added "it"
Line 56: Added "s" to "tends"

Line 56: Removed “the concentrations in the levels near the surface at”
Line 56: Added “under”
Line 56: Added “conditions, and underestimate under higher atmospheric concentration conditions.”
Line 58: Removed “, most probably due to the detection limit of the instrument, and at higher concentrations shows more of an underestimation of”

We also made a number of small edits to improve the readability of the main text:
Line 25: Edited the email address as the old one is no longer viable (change of institute)
Line 71: Added “,”
Line 97: Added “can”
Line 97: Removed “and”
Line 107: Added “,”
Line 110: Added “,”
Line 192: Changed pseudo-lines to Cross-sections
Line 442: Removed “which”
Line 443: Added ”,”
Line 445: Added “,”
Line 462: Removed “.”
Line 463: Removed “Because of”
Line 463: Added “Due to”
Line 608: Removed “and Jacob Siemons (ECCC)”

5. **L39, L48-49: ‘compare well’ These are qualitative terms which do not contain much (if any) information content. Please try to avoid those throughout the manuscript and concentrate on quantitative assessments.**

Removed qualitative terms throughout the document.
Line 30 (all line statements are the positions within the new document): changed “compare well with” to “have a positive”.
Line 301: changed “The overall agreement is good” to “There is an overall agreement”
Line 391: changed “good” to “high”
Line 400: “removed well”
Line 440: changed “agree quite well” to “show agreement”
Line 473: removed “good”
Line 523: changed ‘agree well with” to “ have”
Line 526: changed “agree very well” to “are in agreement”

6. **LL95-96: ‘However, the uncertainty of the satellite observations is still high due to a lack of validation.’ The reasoning is a bit strange: the uncertainty is not caused by lack of validation but rather the knowledge of the uncertainty.**

Edited the sentence to “However, the overall quality of the satellite observations is still highly uncertain due to a lack of validation.”

7. **LL245-246: ‘Do note that on average the observations have a DOFS between 0.9 and 1.1.’ Could you please provide a Figure or numbers of the DOF distribution of all measurements entering the comparison.**

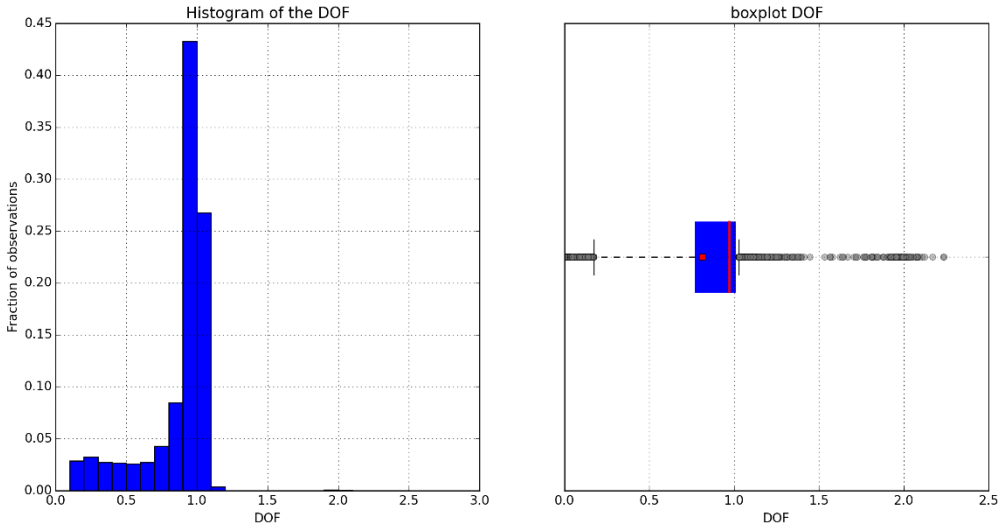

Fig R1.2 Distribution plots of the DOF of all CrIS observations used in this study. The left panel shows the fraction of all observations for each specific DOF range. The right panel shows a boxplot of the same distribution. The box edges are the 25th and 75th percentiles, the red line in the box is the median, the red square is the mean, the whiskers are the 10th and 90th percentiles, and the grey circles are the outlier values outside the whiskers.

Figure R1.2 shows the distribution of the DOF of all measurements. Note that the <0.1 DOF are already removed from this set. ~80 % of the observations have a DOF in between 0.9 and 1.1, with a median of almost 1.0.

8. L246: 'clouds will implicitly be accounted for by the quality control': What is the effect of a partially cloudy field-of-view?

That's a good point. Currently, there is a cloud filter in development to exclude clouded scenes in the future. In our case we remove all observations with a DOF of <0.1 which removes most of the clouded scenes (e.g. thick clouds → no ammonia observed). Besides a reduction in DOF we do not expect further major impacts as mentioned in the TES-NH3 retrieval paper (Shephard et al., 2011). As an example to illustrate potential effects (or the lack there of) we give Fig R1.3. The figure shows a MODIS scene for northern Canada with both visible clouds and fire plumes. The bottom panel shows the calculated CrIS surface NH3 for the same period. As one can observe there are a number of hotspots for NH3 found for the observations surrounding the fires and of the plumes. The optically thick clouds are filtered out by our artificial cut off. The remaining retrieved concentrations for observations with partially covered and by optically thin clouds do not show any strange patterns or alternating high and low retrieved concentrations.

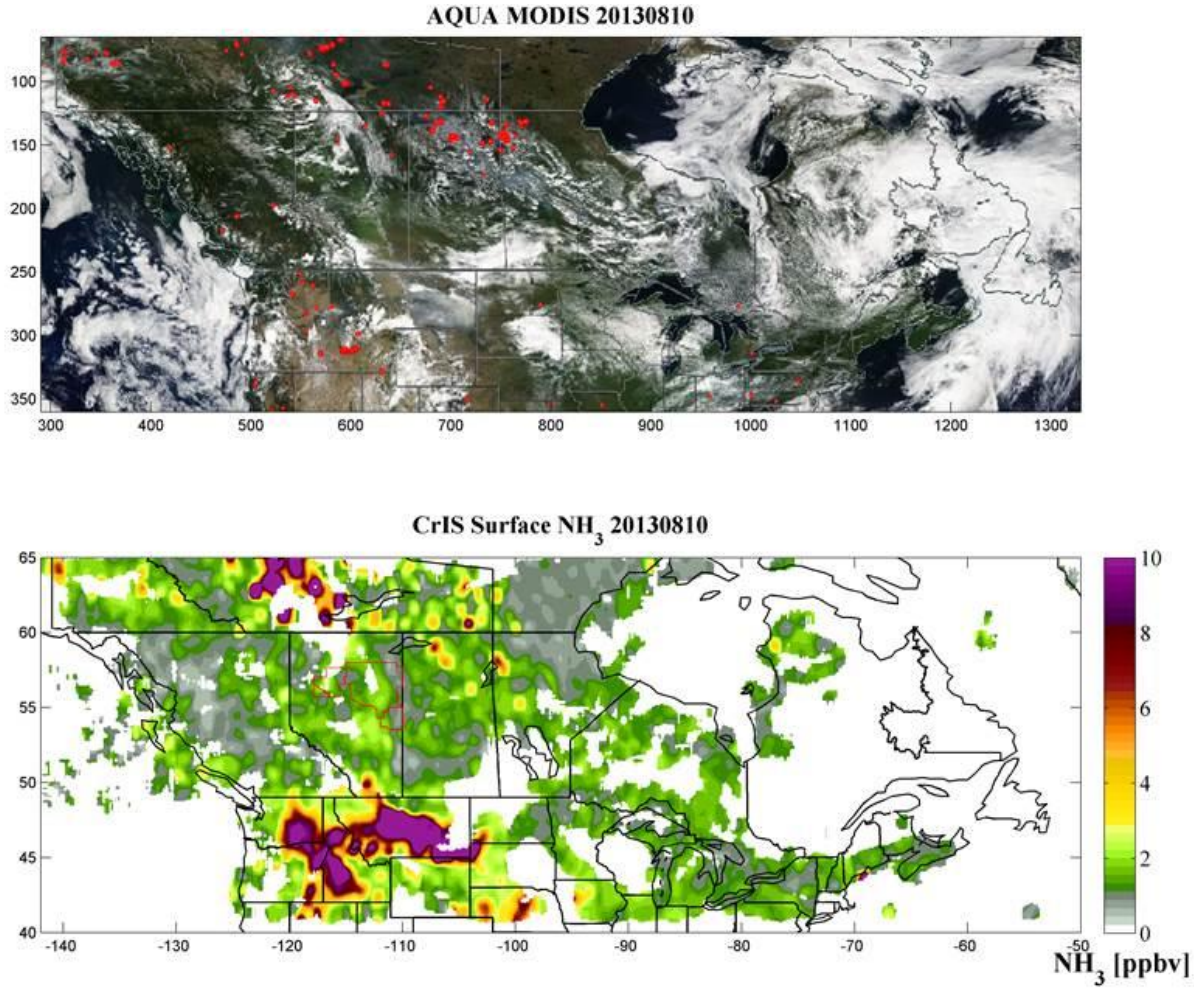

Fig R1.3. Top panel shows the MODIS image over Canada on the 10th of August 2013. Bottom panel shows the retrieved CrIS surface concentrations for the same day.

9. **L301: 'total column comparison': Has this comparison been performed with or without the application of the FTIR-AK as described in chapter 2.5? Since the FTIR is generally better suited for total column retrievals due to its better sensitivity nearer at the ground (where most of the NH3 is present), I doubt that the transformation like in Eq(1), L278 is helpful. Here the better instrument (FTIR) should be transformed to the worse (CrIS) to compare with the CrIS total column amounts. I.e. there should be Figures like Figs. 2 and 3 with the raw data and after the transformation as just described.**

The total column comparison **has been** performed with the application of the FTIR-AK as described in chapter 2.5. In principle we agree that the better instrument should be transformed to the worse (CrIS). However, we wanted to keep the study comparable to the IASI validation study, and thus apply the AVK in the same manner as done in that study. The IASI product does not produce an averaging kernel and thus we cannot apply the satellite observational operator in both cases. Furthermore, to meet readers who would rather see it the other way around, we added alternative figures transforming the FTIR profiles with the CrIS AVK, which are shown in figures A5, A6 and A7.

10. **L318: 'In Toronto, Bremen and Pasadena there is good agreement' In case of Pasadena, I would not call the agreement good. Please also avoid this qualitative terms.**

Changed the qualitative terms as mentioned in edit number 5.. We also added some lines on the results at Pasadena and Wollongong, see edit number 13 for the full description.

Removed, “Pasadena”,

11. L319: ’and low bias in the CrIS total columns for intermediate values’ This seems not to be the case for Bremen.

The only outlier for Bremen is the value that is marked as an outlier by the three sigma filter as used in Figure 2. Furthermore the number of observations is too small for any good statistics.
Added “except for the outlying observation in Bremen, which is marked as an outlier by our three sigma filter used for Figure 2.”

12. L322, Fig. 3: Could you also discuss in the text what the reason for the apparently systematic deviations at Wollongong may be.

There are a number of reasons why the Wollongong bias might look higher than the others. The first is the date of observation. The two comparisons with the highest CrIS to FTIR ratio were both made during the end of November in 2012 when there were multiple fires occurring in the surrounding region (GFED4.1s). Possibly the CrIS footprint covers the plumes from the fire, which was not observed by the FTIR due to an (for us) unfavourable wind direction. The remaining comparisons on average show a MD of ~ 5 x 10^{15}, which is similar to our station wide result. Another explanation might be the difference in observed air masses which can be larger for coastal sites (e.g. Wollongong, and essentially Toronto). Depending on the wind direction there is either clean air coming in from above the lake/ocean which will mean there is a reduction in FTIR observed NH3 while the satellite potentially observes above land. Vice versa observations from the satellite above the ocean/lake can be far lower than the columns observed by the FTIR with a wind direction coming from an inland direction. This heterogeneity is also visible for sites with larger gradients in orography, such as Pasadena and Mexico City.

Line 311: Added “Similarly to Mexico City the comparison also shows an increase in scatter for Pasadena, where the FTIR site is also located on a hill.”

Line 315: Added “In Wollongong, there is less agreement between the instruments. There are two comparisons with large CrIS to FTIR ratios while most of the other comparisons also show a bias for CrIS. For both cases the bias can be explained by the heterogeneity of the ammonia concentrations in the surrounding regions. The two outlying observations were made during the end of November, 2012, which coincides with wild fires in the surrounding region. Furthermore the Wollongong site is located coastally, which will increase the occurrences where one instrument observes clean air from the ocean while the other observes inland air masses.”

13. L331, Fig. 4: ‘show the standard deviation for each value’ Is this the standard deviation of the distribution of the differences or the standard error of the mean difference (i.e. the former divided by sqrt(number of values))? The latter should (also) be shown to detect any significant measurement bias.

Fig 4 showed the standard deviation of the distribution of the differences. As noted in the reply to Referee number 2 we edited the figure to show the 95% confidence interval i.e. ~2x standard error.

14. LL379-380: ‘along with the shorter atmospheric path lengths for observations from the ground-based solar-pointing FTIR’ Could you explain, why the FTIR path length is shorter compared to the satellite? Is this always the case?

In principle the atmospheric path length should be more or less similar. The path length of both instruments vary per location of the site, time of day and field of view of the satellite, but the difference should be more or less near zero.

Line 379: Removed sentence

15. **LL377-385: As already mentioned, for this discussion the total column operator or the partial column(number density) AK would be interesting. As the FTIR is more sensitive down to the ground level than the satellite where there are highest concentrations of NH3, the satellite retrieval should be determined by the a-priori there. So the higher column amounts may be produced by higher a-priori values at the ground.**

That's a good point but for the fact that the application of the observational operator should reduce the effects of the difference in sensitivity and a-priori choice. Any remaining effect of the a-priori is hard to judge without a repeat of the retrieval. What potentially can be done to further reduce the influence of the a-priori is switching out the a-priori. For a number of examples of the a-priori switch, we point you to figures R2.1 to R2.4 in our reply to Referee number 2.

16. **L550: 'improvements to the NH3 line spectroscopy to reduce the uncertainty coming from this error source' Could you give the information if the CrIS retrieval also uses Hitran2012, like the FTIR?**

The CrIS retrieval also uses HITRAN 2012.

Added:
"and uses the HITRAN database (Rothman et al., 2014) for its spectral lines"

Technical comments:
L566, Fig. A1: the arrangement of the panels in the figure is transposed with respect to the description in the caption.
Good catch,
L566 Fig. A1 caption, changed to: "Error profiles for each of the error terms. The left panels show the random errors, the right panels the systematic errors. The top two panels show the error in VMR. The bottom panels show the errors in partial column layers [molecules cm^{-2}]. (See Figure A.2 for the same figure but with the errors relative to the final VMR and partial columns per layer)"

L571, Fig. A2: same problem as in Fig. A1. Moreover, the top and the bottom row seem to show identical data.
It is correct that the top and bottom row are showing identical data as the error is initially derived for the VMR value and subsequently applied to the partial columns.

L571 Fig. A2 caption, changed to: "Relative error profiles for each of the error terms. The left panels show the Random errors, right panels the Systematic errors. All four panels show the error in a fraction of the original unit used in Figure A1. (See Figure A.1 for the same figure but with the absolute errors)"

References.
Shephard, M. W., Cady-Pereira, K. E., Luo, M., Henze, D. K., Pinder, R. W., Walker, J. T., Rinsland, C. P., Bash, J. O., Zhu, L., Payne, V. H., and Clarisse, L.: TES ammonia retrieval strategy and global observations of the spatial and seasonal variability of ammonia, Atmos. Chem. Phys., 11, 10743-10763, doi:10.5194/acp-11-10743-2011, 2011.

van der Werf, G. R., Randerson, J. T., Giglio, L., van Leeuwen, T. T., Chen, Y., Rogers, B. M., Mu, M., van Marle, M. J. E., Morton, D. C., Collatz, G. J., Yokelson, R. J., and Kasibhatla, P. S.: Global fire emissions estimates during 1997–2015, Earth System Science Data Discussions, doi:10.5194/essd-2016-62, in review, 2017.

Reply to comments, Referee #2

We would like to thank Referee #2 for his/her time, constructive and helpful comments and suggestions. Throughout the document (R1 stands for reviewer 1, and figures named R1.x point to the x'th figure in "Reply to comments, Referee #1)

General Comments:

1. **One particular issue that could hamper the interpretation of the results is the potentially limited information content captured by the CrIS retrievals. The current DOFS cut off is taken at >0.1, which entails that some measurements are/could be heavily dominated by the a-priori. The authors allude that particularly measurements with low NH3 concentrations could be effected. One way to at least give some information on this is to replot Fig2, whereby each measurement is coloured related to its (average) DOFS.**

The **artificial** DOF **cut off** was chosen to remove observations without information. We added colouring to the scatterplot indicating the average DOF for each CrIS observation, with the colour bar ranging from 0.1 to more than 1.1. See the reply to the comments of ref #1 for a distribution of the DOF for all observations used in this study.

Added "The colouring on the scatter indicates the mean DOF of each the CrIS coincident data." to the caption of Figure 2.

2. **Another way to test whether observed differences between CrIS and FTIR are driven by differences in a-priori rather than the actual retrieval, is to (prior to mapping CrIS to FTIR –see eq(1)) conform the CrIS retrieval to the FTIR a-priori as in Rodgers (2000): x(CrIS,ftir apriori corrected)=x(CrIS) +[A(CrIS)-I]*[apriori(CrIs)-apriori(ftir)]**

That is a great question and it is something we have tried before submitting. A posteriori switching out the CrIS a-priori for the FTIR a-priori essentially brings us closer to what we want, validating just the observations without an effect from the a-priori. The problem however is the non-linearity in the retrievals (Kulawik et al., 2008). The resulting retrieved profile is not always near/comparable to the initial a-priori shape and amplitude (which in itself shows that the initial choice of a-priori does not greatly influence the retrieval), which makes an a posteriori switch of the a-priori profile troublesome. Without a repeat of the CrIS retrievals it is not possible to distinguish between the effect of the a priori on the retrieval and the effect of the a posteriori switch. The study by Kulawik et al., (2008) showed that the effect does not have to be major as long as the a priori is representative of the final retrieved profile. This however is not always the case in our retrievals. To illustrate we give a number of examples. Fig R2.1 to R2.4 show the effect for a range of atmospheric ammonia concentrations at a variety of sites, starting with situations with medium to large concentrations for Pasadena (Fig R2.1, which is Figure 5 in the main manuscript), Bremen (Fig R2.2) and Toronto(Fig R2.3). Furthermore we added a figure showing the situation when there is not much ammonia i.e. Wollongong (Fig R2.4). In the case of Pasadena the difference is only small with a few percent change in the concentrations of the individual layers. For Bremen the difference is larger near the surface, corresponding to the higher concentration levels. Especially near the surface the concentration change is high following the abrupt difference in the a priori shape, which does not have the sharp peak like the CrIS a priori. In the case of Toronto the effect is in the order of 10%, although concentrations around 750hPa, turn negative. In the Wollongong example the relative difference is large, as the retrieved concentrations are low. The large difference shows that a change of 1-2 ppb in the a priori shape and amplitude cannot be seen as a small enough difference to permit an a posteriori change.

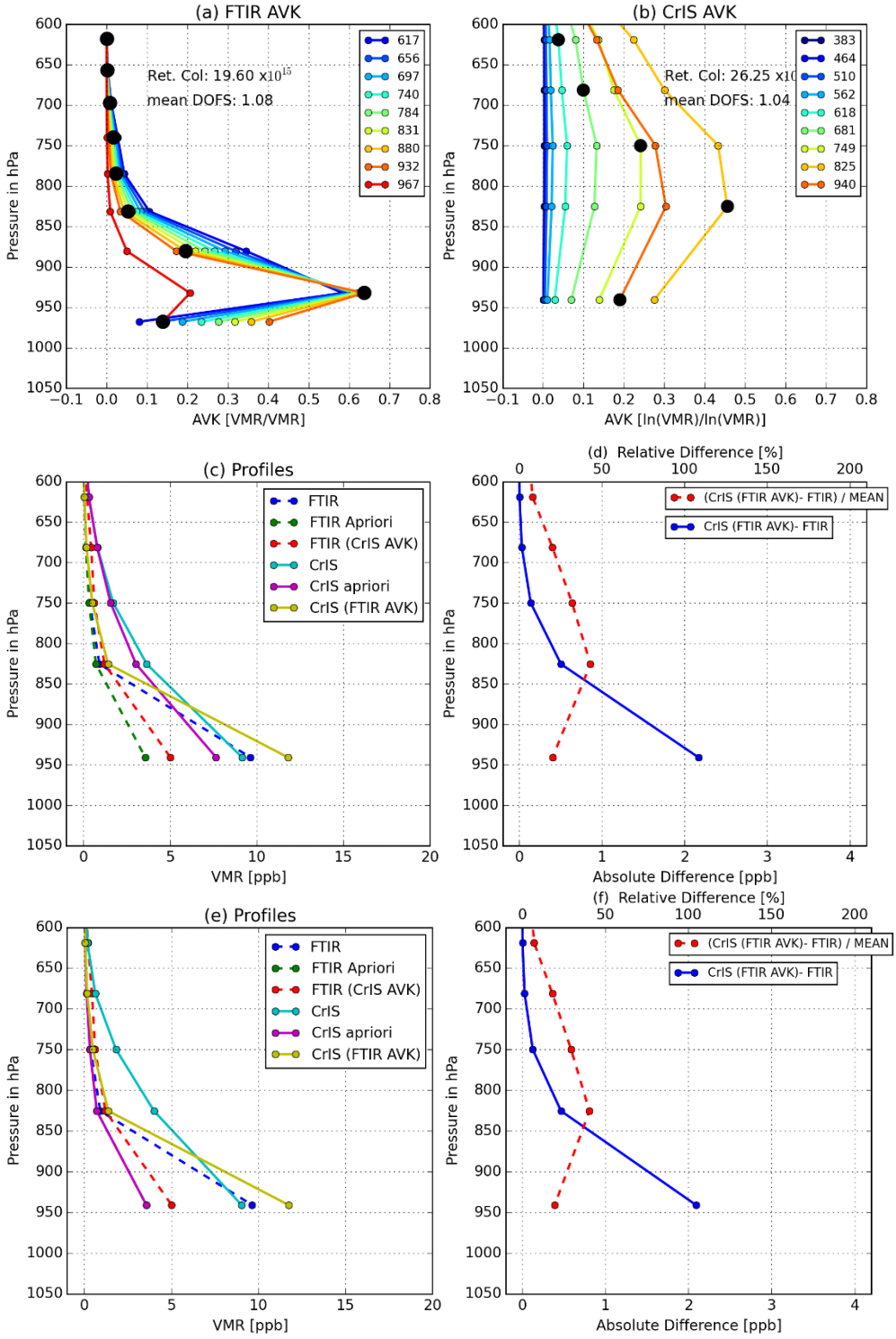

Fig R2.1. Example of the effect of switching out the CrIS a priori for the FTIR a priori to the CrIS Retrieved profile, for an FTIR profile matched with a CrIS profile measured around the **Pasadena** site. For the full figure caption see Figure 5 in the main manuscript. Panel (e) shows is a copy of panel (c) but now with the CrIS a priori switched out for the FTIR a priori. Similarly (f) shows the same as panel (d) after switching out the CrIS a priori for the FTIR a priori.

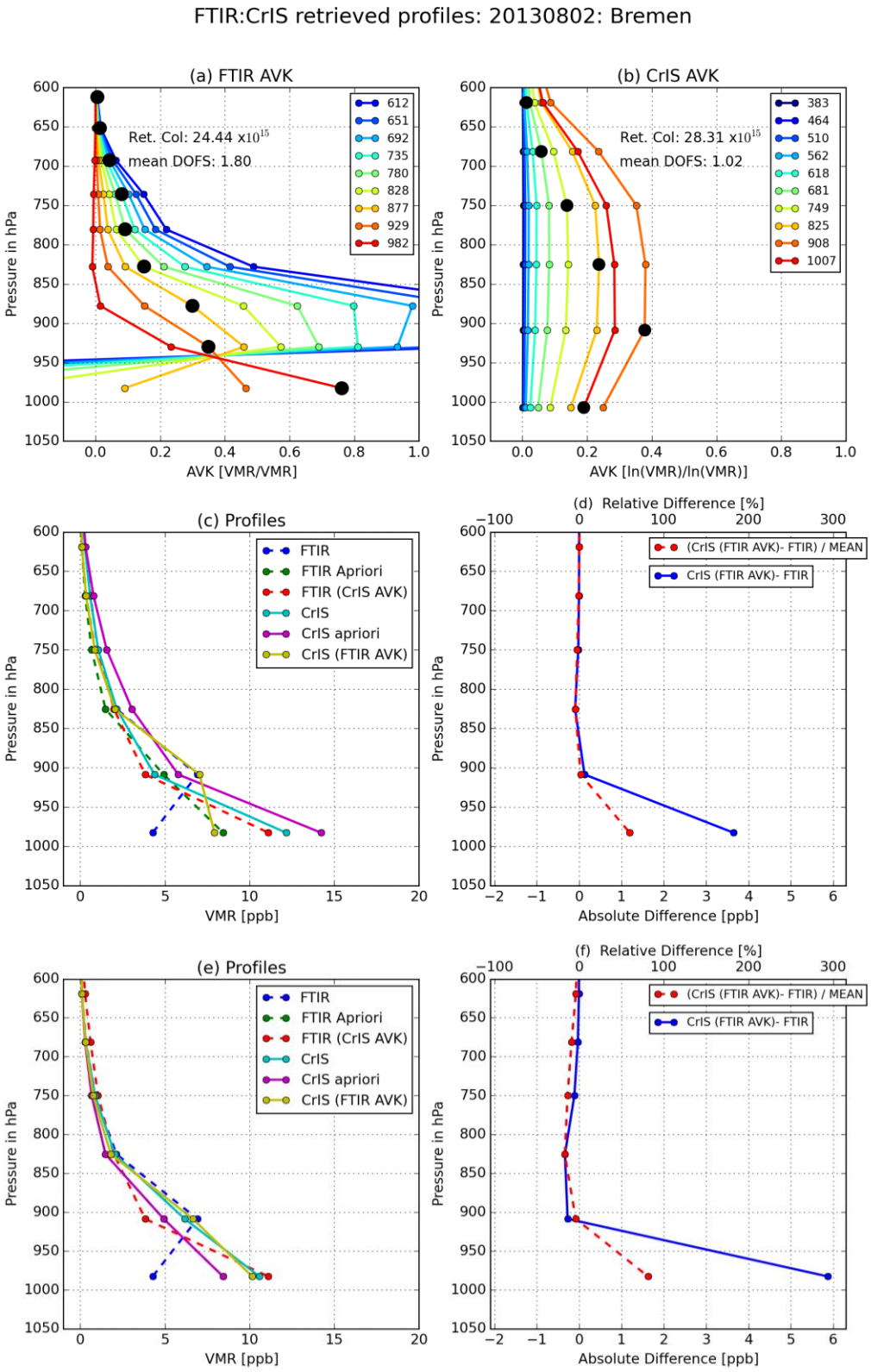

Fig R2.2. Example of the effect of switching out the CrIS a priori for the FTIR a priori to the CrIS Retrieved profile, for an FTIR profile matched with a CrIS profile measured around the **Bremen** site. For the full figure caption see Figure 5 in the main manuscript. Panel (e) shows is a copy of panel (c) but now with the CrIS a priori switched out for the FTIR a priori. Similarly (f) shows the same as panel (d) after switching out the CrIS a priori for the FTIR a priori.

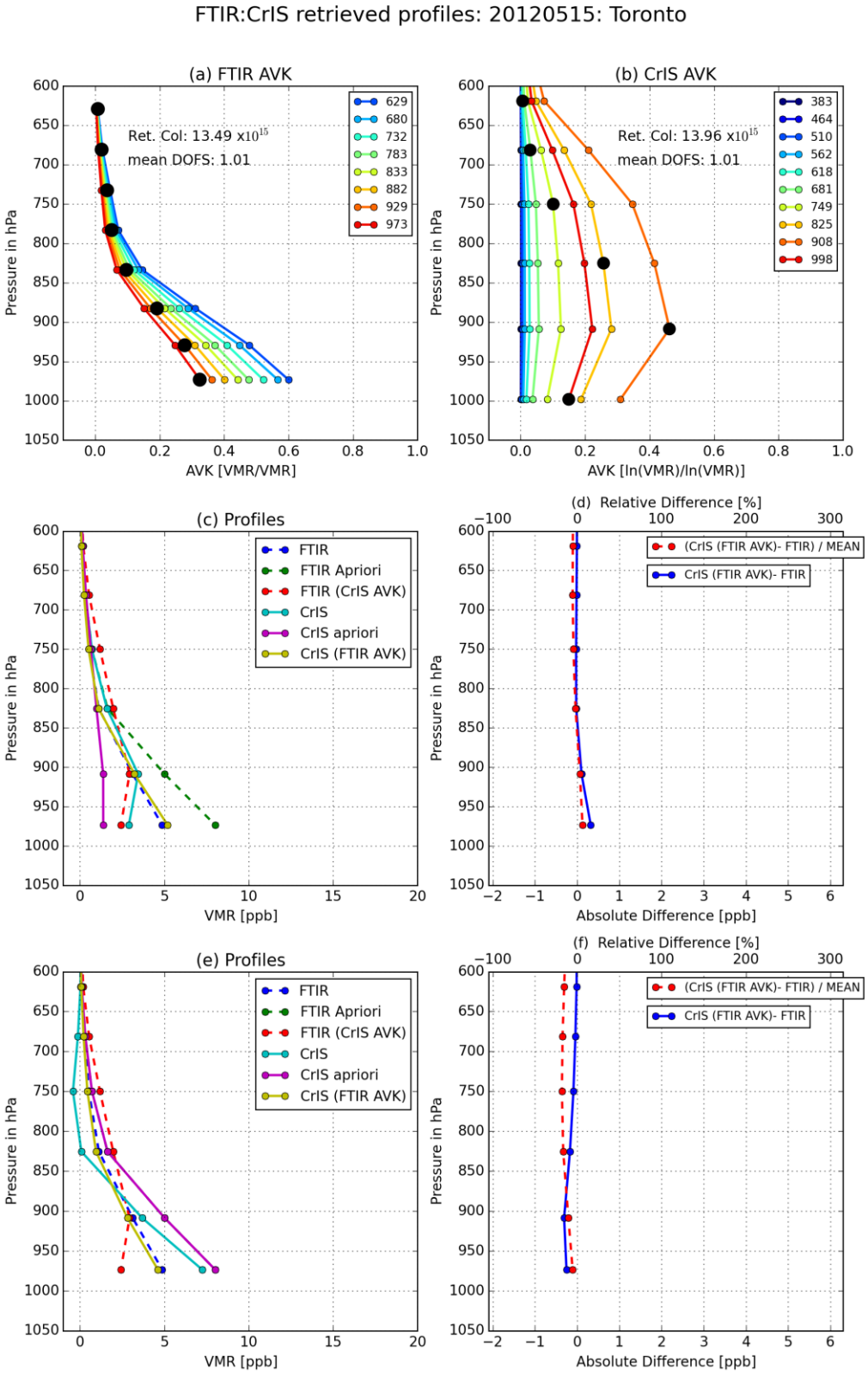

Fig R2.3. Example of the effect of switching out the CrIS a priori for the FTIR a priori to the CrIS Retrieved profile, for an FTIR profile matched with a CrIS profile measured around the **Toronto** site. For the full figure caption see Figure 5 in the main manuscript. Panel (e) shows is a copy of panel (c) but now with the CrIS a priori switched out for the FTIR a priori. Similarly (f) shows the same as panel (d) after switching out the CrIS a priori for the FTIR a priori.

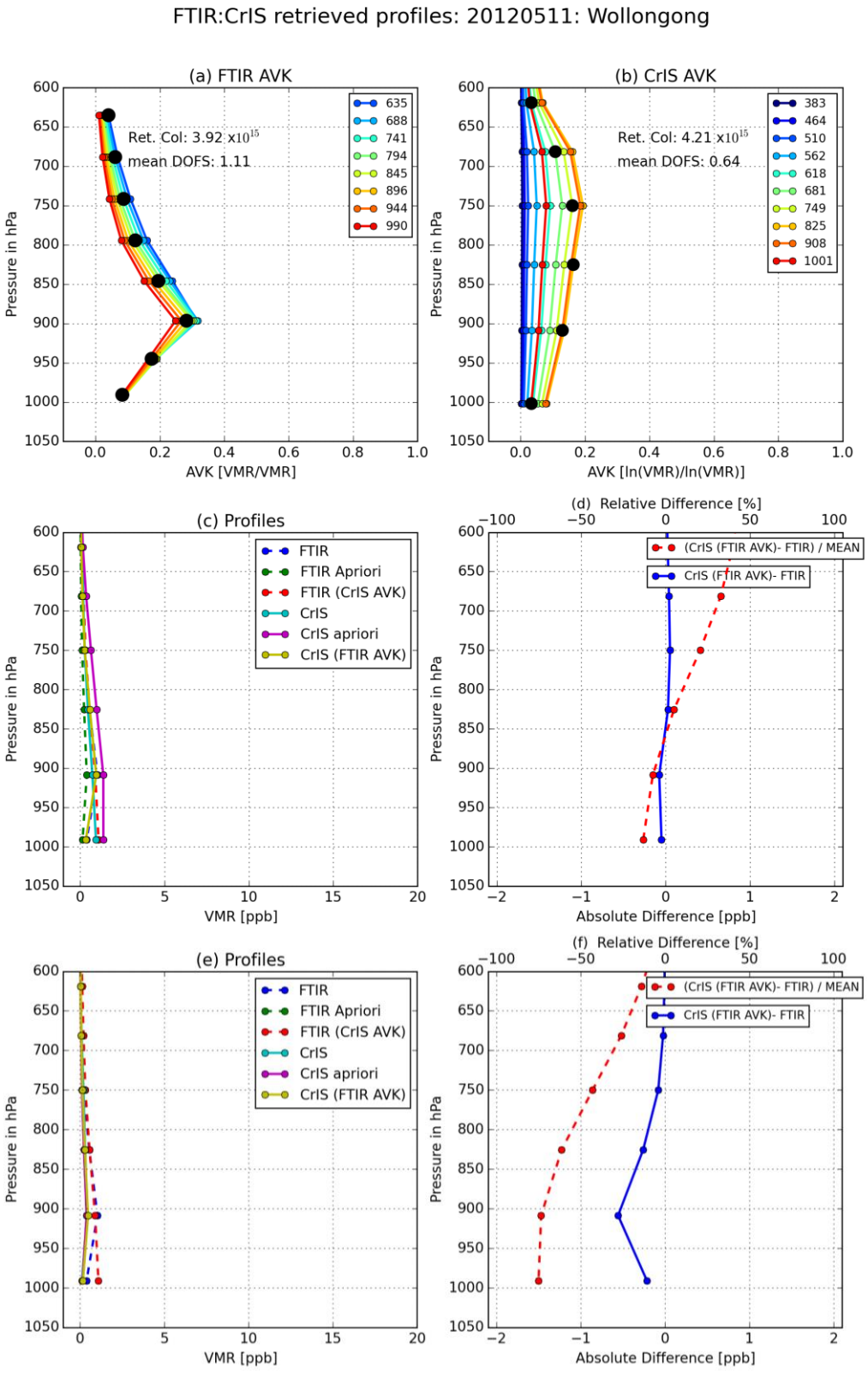

Fig R2.4. Example of the effect of switching out the CrIS a priori for the FTIR a priori to the CrIS Retrieved profile, for an FTIR profile matched with a CrIS profile measured around the **Wollongong** site. For the full figure caption see Figure 5 in the main manuscript. Panel (e) shows is a copy of panel (c) but now with the CrIS a priori switched out for the FTIR a priori. Similarly (f) shows the same as panel (d) after switching out the CrIS a priori for the FTIR a priori.

3. **In any case, the authors need to look deeper into the possible effects of the DOFS on the bias.**

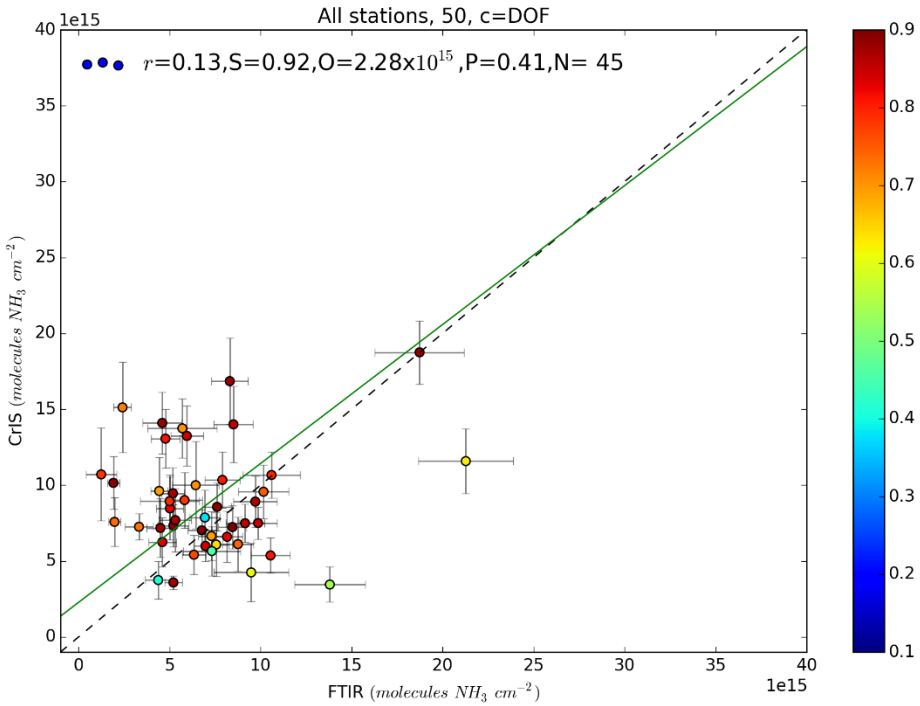

Fig R2.5. Correlation between the FTIR and CrIS total columns using the coincident data from all measurement sites for all CrIS observations with a mean DOF < 0.9. The horizontal and vertical bars show the total error on each FTIR and CrIS observation. The colouring on the scatter indicates the mean DOF of each the CrIS coincident data. The trend line shows the results of the regression analysis.

We looked into the effects of the DOF, but decided to not put any further emphasis on it in the main manuscript. Essentially most (>80%) of the observations have a DOF between 0.9 – 1.1. From the remaining 20 % the larger number are above >0.7 leaving a small set of observations (~10%) with a DOF <0.7. Figure R2.5 shows a scatterplot similar to Figure 2 in the main manuscript but now with only observations with a DOF <0.9. As one can see there is no clear relation visible between the amount of scatter and the DOF. About 20% of the observations (N=45 in total) used for Figure 2 have a DOF < 0.9. Table R1 shows the mean difference and mean relative difference for the observations with a DOF<0.9. For comparability we added the full set of observations to the table, coloured in red. The observations with small DOFs usually are observations with a relatively low ammonia concentration. This makes that we can only really compare the lower range of total columns to our earlier results as there are only 6 observations with a total column > 10 x 10^{15} molecules cm^{-2}. The observations smaller than > 10 x 10^{15} molecules cm^{-2} have a MD of 2.6 with a std of 4.1 which is comparable to the complete set with 3.3 (std = 4.1). Similarly the MRD is 33.0 %(std = 54.9%) which is also in the same range as the original set's 30.2% (std = 38.0%)).

Table R1. Results of the total column comparisons of the FTIR to CrIS for observations with a DOF<0.9. N is the number of averaged total columns, MD is the mean difference [10^{15} molecules cm^{-2}], MRD is the mean relative difference [frac, in %]. Value for the complete set used in Table 3 and Fig 4 are given in red. Take note that the combined value N does not add up with all the separate sites as observations have been included for FTIR total columns > 5 x 10^{15} molecules cm^{-2}.

Retrieval	Column total range in molecules cm^{-2}	N	MD in 10^{15} (1σ)	MRD in % (1σ)	FTIR mean in 10^{15} (1σ)
CrIS-NH3	< 10.0 x 10^{15}	39	2.6 (4.1)	33.0 (54.9)	6.1 (2.2)
CrIS-NH3	>= 10.0 x 10^{15}	6	-4.3 (4.4)	-41.6 (44.3)	14.2 (4.3)
CrIS-NH3	< 10.0 x 10^{15}	93	3.3 (4.1)	30.2 (38.0)	7.5 (1.5)
CrIS-NH3	>= 10.0 x 10^{15}	109	0.4 (5.3)	-1.39 (34.4)	16.7 (8.5)

A few outlying values are observed in Fig R2.5 which show more of a dependency to location than to DOF, as illustrated in Fig R2.6. All of the larger retrieved total columns (both FTIR and CrIS, >10 x 10^{15} molecules cm^{-2}) are observations from the Toronto measurement site. As noted in the main manuscript the Toronto results are influenced by the local conditions, which increase the heterogeneity in the region. The site is located within the city, further away from the main sources surrounding the city. Furthermore Toronto is located at the edge of Lake Ontario, which increases the differences as for days with wind originating from the south one can expect clean air observed by the FTIR, where the satellite observes the emitted ammonia of the sources outside the city. Similarly for conditions with wind from the north one can expect

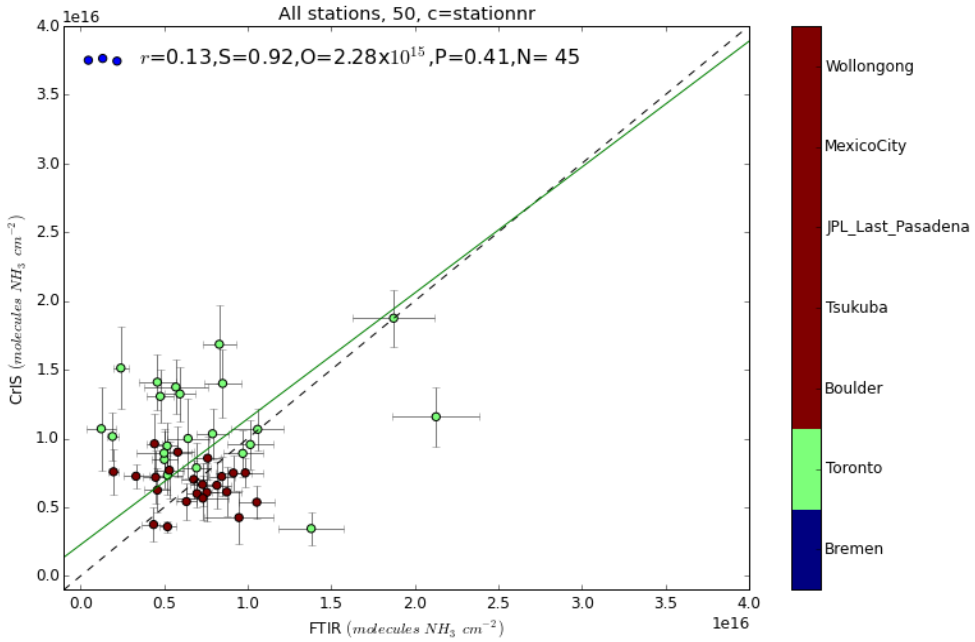

Figure R2.6. Correlation between the FTIR and CrIS total columns using the coincident data from all measurement sites for all CrIS observations with a mean DOF < 0.9. The horizontal and vertical bars show the total error on each FTIR and CrIS observation. The colouring on the scatter indicates the FTIR measurement site. The trend line shows the results of the regression analysis.

4. **A second general comment is the error analysis which could be improved. The document either misses a general statement that all presented errors correspond with the 1-sigma standard deviation or it sometimes needs to be more specific when it uses the term 'error' as it sometimes relates to the standard deviation on the bias and sometimes on the bias itself. That said, 1-sigma standard deviations often tell little with regards to the statistical significance of an observed difference. For instance one claim made by the authors is that in the 0.5-1.0 e16 bin CrIS is significantly higher. This is likely to be true but from the article alone I cannot verify this. In Figure 4 the observed binned biases are shown with their standard deviations. A much better metric to**

show statistical significance would be the 95 or 99% confidence interval on the mean. This goes for all metrics where statistical significance is claimed or investigated.

Some parts are indeed confusing. We cleaned up the text and added a few sentences to clarify what error we are talking about. We define two types of errors, 1. Estimated errors: FTIR & CrIS retrieval & prior knowledge and 2. the actual errors i.e. the mean and mean relative differences that come out of the comparison. In the case of Figure 4, we edited the figure to include the 95 % confidence level as the number of observations were not included. Throughout the text we left it at standard deviation. Optionally one could calculate it directly from the standard deviation and the number of observations.

Line 296: edited caption, "total estimated error"

Line 305: removed "significantly"

Line 363, 365: added , N = 229)

Line 365, 364: added "std =" in between brackets"

Line 403: added "estimated" to "estimated error"

Line 460: changed "bias" to "actual error"

Line 538: added "estimated"

Line 527, 529, 530, 531: added "std =" in between brackets

Line 582: changed "bias" to "actual error"

Caption Fig 4. Added "The number of observations in each set is shown in the bottom panel."

Specific comments:

5. **L155: A list of the dominant interfering species would be useful here**

L155: Changed "i.e. interfering species" to "(i.e. major interfering species such as H_2O, CO_2, and O_3)"

6. **L165: A representation of the used collocation area would be useful in this figure**

Adjusted Figure 1 to include 2 circles with radii of 25 and 50 km.

Added a second sentence to the caption of figure 1: "The two circles show the collocation area when for radii of 25 and 50 km."

7. **L305: show the error (be more specific= standard deviation is better)**

L305: Added "total" to indicate it is not a standard deviation of the observations. The bars indicate the mean total error of the combined observations.

8. **L319: Pasadena looks worse at elevated values**

L319: Removed Pasadena.

9. **L320: in, and low bias ("in" is obsolete)**

L320: removed "in"

10. **L465: red diamond -> red square**

Changed “diamond” to “square in all bar plot figures.

11. **L468: Summary of the errors. . . Could be interpreted as the uncertainty on the biases, not the actual absolute and relative bias**

Caption figure 7: Changed “summary of the errors” to “Summary of the absolute and relative bias”.

L580: Caption Fig. A5. Similarly changed to “Summary of the absolute and relative bias”

Author comment

We made a number of small edits to the text to improve the readability of the manuscript. The changes made are the following;

Added a figure to the appendix to improve comparability of the results of the IASI and CrIS retrievals.

Line 366: added "To put the results of this study into perspective of the IASI-LUT and IASI-NN products we added Figure A1 to the Appendix, which shows the total column comparison for both products."

Inserted caption:

"Figure A1. Correlation between the FTIR and the IASI-LUT (left, blue) and IASI-NN (right, red) total columns using the coincident data from all measurement sites. The horizontal and vertical bars show the total estimated error on each FTIR and CrIS observation. A three sigma outlier filter was applied to the IASI-LUT dataset and the same observations were removed from the IASI-NN set. Contrary to the earlier study by Dammers et al., (2016a) no thermal contrast filter was applied to the dataset."

We changed the numbering of the other appendix figures to match the new order.

Shortened and slightly edited the abstract for readability

Line 44: Added "(<1.0x1016 molecules cm-2)"
Line 45: Removed "and the FTIR total columns are smaller than 1.0x1016 molecules cm-2,"
Line 46: Removed "are small with CrIS showing"
Line 47: Added "show"
Line 47: Removed "around +2.4 x 1015 (standard deviation = ±5.5 x 1015) molecules cm-2, which corresponds to a relative difference of ~+50% (std = ±100 %)."
Line 48: Added "The CrIS and FTIR profile comparisons differences are mostly within the range of the estimated retrieval uncertainties single level retrieved profile values showing average difference in the range of ~20 to 40%"
Line 50: Removed "for these comparisons"
Line 51: Added "into the boundary layer that typically peaks at"
Line 51: Removed "to"
Line 52: Added "(~1.5 km)"
Line 52: Removed "and"
Line 52: Removed "retrieved profiles also compare well with the"
Line 53: Added "is"
Line 53: Removed "of"
Line 53: Added "std ="
Line 53 Added ","
Line 53 Removed "and a"
Line 53: Added "%"
Line 53: Added "std ="
Line 54: Removed "Most of the absolute and relative profile comparison differences are in the range of the estimated retrieval uncertainties. However, t"
Line 56: Added "At the surface, where CrIS typically has lower sensitivity,"
Line 55: Removed "he CrIS retrieval does"
Line 55: Added "it"
Line 56: Added "s" to "tends"
Line 56: Removed "the concentrations in the levels near the surface at"
Line 56: Added "under"
Line 56: Added "conditions, and underestimate under higher atmospheric concentration conditions."
Line 58: Removed ", most probably due to the detection limit of the instrument, and at higher concentrations shows more of an underestimation of"

Further small edits readability in main text

Line 25: Edited the email address as the old one is no longer viable (change of institute)
Line 71: Added “,”
Line 97: Added “can”
Line 97: Removed “and”
Line 107: Added “,”
Line 110: Added “,”
Line 192: Changed pseudo-lines to Cross-sections
Line 442: Removed “which”
Line 443: Added ”,”
Line 445: Added “,”
Line 462: Removed “.”
Line 463: Removed “Because of”
Line 463: Added “Due to”
Line 608: Removed “and Jacob Siemons (ECCC)”

Validation of the CrIS Fast Physical NH_3 Retrieval with ground-based FTIR

Enrico Dammers[1], Mark W. Shephard[2], Mathias Palm[3], Karen Cady-Pereira[4], Shannon Capps[5*], Erik Lutsch[6], Kim Strong[6], James W. Hannigan[7], Ivan Ortega[7], Geoffrey C. Toon[8], Wolfgang Stremme[9], Michel Grutter[9], Nicholas Jones[10], Dan Smale[11], Jacob Siemons[2], Kevin Hrpcek[12], Denis Tremblay[13], Martijn Schaap[14], Justus Notholt[3], Jan Willem Erisman[1,15]

1. Cluster Earth and Climate, Department of Earth Sciences, Vrije Universiteit Amsterdam, Amsterdam, the Netherlands
2. Environment and Climate Change Canada, Toronto, Ontario, Canada
3. Institut für Umweltphysik, University of Bremen, Bremen, Germany
4. Atmospheric and Environmental Research (AER), Lexington, Massachusetts, USA
5. Department of Mechanical Engineering, University of Colorado, Boulder, Colorado, USA
6. Department of Physics, University of Toronto, Toronto, Ontario, Canada
7. NCAR, Boulder, Colorado, United States
8. Jet Propulsion Laboratory, California Institute of Technology, Pasadena, California, USA
9. Centro de Ciencias de la Atmósfera, Universidad Nacional Autónoma de México, Mexico City, Mexico
10. University of Wollongong, Wollongong, Australia
11. National Institute of Water and Atmosphere, Lauder, New Zealand
12. University of Wisconsin-Madison Space Science and Engineering Center (SSEC), Madison, Wisconsin, USA.
13. Science Data Processing, Inc., Laurel, MD, United States
14. TNO Built Environment and Geosciences, Department of Air Quality and Climate, Utrecht, the Netherlands
15. Louis Bolk Institute, Driebergen, the Netherlands

*Now at Civil, Architectural, and Environmental Engineering Department, Drexel University, Philadelphia, Pennsylvania, USA

Correspondence to: E. Dammers (enrico.dammers@~~vu~~gmail.~~nl~~com)

Abstract

~~Global reactive nitrogen emissions into the air have increased to unprecedented levels. Limiting the loss of reactive nitrogen into the environment is one of the major challenges for humankind. At the current levels ammonia (NH_3) is a threat to both the environment and human health. However, relatively little is known about the total nitrogen budget and distribution around the world, due in part to the sparseness of observations over most of the globe. Recent advances in the capabilities of measuring NH_3 with satellite instruments have improved the situation with sensors such as the Infrared Atmospheric Sounding Interferometer (IASI) and the Cross-Track Infrared Sounder (CrIS) making twice daily observations with global coverage. However, these require validation to be truly useful, and one of the main challenges in the validation of the satellite NH_3 profile and total column data products is the scarcity of measurements that can be directly compared.~~ Presented here is the validation of the CrIS Fast Physical Retrieval (CFPR) NH_3 column and profile measurements using ground-based Fourier Transform Infrared (FTIR) observations. We use the total columns and profiles from seven FTIR sites in the Network for the Detection of Atmospheric Composition Change (NDACC) to validate the satellite data products. The overall FTIR and CrIS total columns ~~compare well with~~have a positive ~~a~~ correlation of r = 0.77 (N=218) with very little bias (a slope of 1.02). Binning the comparisons by total column amounts, for concentrations larger than 1.0 x 10^{16} molecules cm^{-2}, i.e. ranging from moderate to polluted conditions, the relative difference is on average ~ 0 - 5% with a standard deviation of 25-50%, which is comparable to the estimated retrieval uncertainties in both CrIS and the FTIR. For

Formatted: Justified

the smallest total column range (<1.0x10^{16} molecules cm^{-2}) where there are a large number of observations at or near the CrIS noise level (detection limit) ~~and the FTIR total columns are smaller than 1.0x10^{16} molecules cm^{-2},~~ the absolute differences between CrIS and the FTIR total columns ~~are small with CrIS showings~~show a slight positive column bias ~~around +2.4 x 10^{15} (standard deviation = 5.5 x 10^{15}) molecules cm^{-2}, which corresponds to a relative difference of ~+50% (std = 100 %).~~. The CrIS and FTIR profile comparisons differences are mostly within the range of the estimated retrieval uncertainties single level retrieved profile values, showing average differences in the range of ~20 to 40%. The CrIS retrievals ~~for these comparisons~~ typically show good vertical sensitivity down into the boundary layer that typically peaks at~~to~~ ~850 hPa (~1.5 km), ~~and~~ at this level the ~~the retrieved profiles also compare well with the~~ median absolute difference ~~of~~is 0.87 (std = ±0.08) ppb ~~and a,~~ corresponding to a median relative difference of 39% (std = ±2%)~~%~~. Most of the absolute and relative profile comparison differences are in the range of the estimated retrieval uncertainties. ~~However, the CrIS retrieval does~~ At the surface, where CrIS typically has lower sensitivity, it tends to overestimate ~~the concentrations in the levels near the surface at~~ under low concentrations conditions, and underestimate under higher atmospheric concentration conditions~~, most probably due to the detection limit of the instrument, and at higher concentrations shows more of an underestimation of the concentrations in these lower levels.~~.

1. Introduction

The disruption of the nitrogen cycle by the human creation of reactive nitrogen has created one of the major challenges for humankind (Rockström et al., 2009). Global reactive nitrogen emissions into the air have increased to unsurpassed levels (Fowler et al., 2013) and are currently estimated to be four times larger than pre-industrial levels (Holland et al., 1999). As a consequence the deposition of atmospheric reactive nitrogen has increased causing ecosystems and species loss (Rodhe et al 2002; Dentener et al., 2006; Bobbink et al., 2010). Ammonia (NH_3) as fertilizer is essential for agricultural production and is one of the most important reactive nitrogen species in the biosphere. NH_3 emission, atmospheric transport, and atmospheric deposition are major causes of eutrophication and acidification of soils and water in semi-natural environments (Erisman et al., 2008, 2011). Through reactions with sulphuric acid and nitric acid, ammonium nitrate and ammonium sulphate are formed, which embody up to 50% of the mass of fine mode particulate matter ($PM_{2.5}$) (Seinfeld and Pandis., 1988; Schaap et al., 2004). $PM_{2.5}$ has been associated with various health impacts (Pope et al., 2002; 2009). At the same time, atmospheric aerosols impact global climate directly through their radiative forcing effect and indirectly through the formation of clouds (Adams et al., 2001; Myhre et al., 2013). By fertilizing ecosystems, deposition of NH_3 and other reactive nitrogen compounds also plays a key role in the sequestration of carbon dioxide (Oren et al., 2001).

Despite the significance and impact of NH_3 on the environment and climate, its global distribution and budget are still relatively uncertain (Erisman et al., 2007; Clarisse et al., 2009; Sutton et al., 2013). One of the reasons is that in-situ measuring of atmospheric NH_3 at ambient levels is complex due to the sticky nature and reactivity of the molecule, leading to large uncertainties and/or sampling artefacts with the currently used measuring techniques (von Bobrutzki et al., 2010; Puchalski et al., 2011). Measurements are also very sparse. Currently, observations of NH_3 are mostly available in north-western Europe and central North America, supplemented by a small number of observations made in China (Van Damme et al., 2015b). Furthermore, there is a lack of detailed information on its vertical distribution as only a few dedicated airborne measurements are available (Nowak et al., 2007, 2010; Leen et al., 2013, Whitburn et al., 2015, Shephard et al., 2015). The atmospheric lifetime of NH_3 is rather short, ranging from hours to a few days. In summary, global emission estimates have large uncertainties. Estimates of regional emissions attributed to source types different from the main regions are even more uncertain due to a lack of process knowledge and atmospheric levels (Reis et al., 2009).

Over the last decade the developments of satellite observations of NH_3 from instruments such as the Cross-track Infrared Sounder (CrIS, Shephard and Cady-Pereira, 2015), the Infrared Atmospheric Sounding Interferometer (IASI, Clarisse et al., 2009; Coheur et al., 2009; Van Damme et al., 2014a), the Atmospheric Infrared Sounder (AIRS, Warner et al., 2016), and the Tropospheric Emission Spectrometer (TES, Beer et al., 2008; Shephard et al., 2011) show potential to improve our understanding of the NH_3 distribution. Recent studies show the global distribution of NH_3 measured at a twice daily scale (Van Damme et al., 2014a, Van Damme et al., 2015a) ~~and~~ can reveal seasonal cycles and distributions for regions where measurements were unavailable until now. Comparisons of these observations to surface observations and model simulations, show underestimations of the modelled NH_3 concentration levels, pointing to underestimated regional and national emissions (Clarisse et al.,

2009; Shephard et al., 2011; Heald et al., 2012; Nowak et al., 2012; Zhu et al., 2013; Van Damme et al., 2014b; Lonsdale et al., 2016; Schiferl et al., 2014, 2016; Zondlo et al., 2016). However, the overall ~~uncertainty~~ quality of the satellite observations is still highly uncertain due to a lack of validation. The few validation studies showed a limited vertical, spatial and or temporal coverage of surface observations to do a proper uncertainty analysis (Van Damme et al., 2015b; Shephard et al., 2015; Sun et al., 2015). A recent study by Dammers et al. (2016a) explored the use of Fourier transform infrared (FTIR-NH_3, Dammers et al., 2015) observations to evaluate the uncertainty of the IASI-NH_3 total column product. The study showed the good performance of the IASI-LUT (Look up table, LUT, Van Damme et al., 2014a) retrieval with a high correlation ($r \sim 0.8$), but indicated an underestimation of around 30% due to potential assumptions of the shape of the vertical profile (Whitburn et al., 2016, IASI-NN (Neural Network, NN)), uncertainty in spectral line parameters and assumptions on the distributions of interfering species. The study showed the potential of using FTIR observations to validate satellite observations of NH_3, but also stressed the challenges of validating retrievals that do not provide the vertical measurement sensitivity, such as the IASI-LUT retrieval. Since no IASI satellite averaging kernels are provided for each retrieval, and thus no information is available on the vertical sensitivity and/or vertical distribution of each separate observation, it is hard to determine the cause of the discrepancies between both observations.

The new CrIS Fast Physical Retrieval (Shephard and Cady-Pereira, 2015) uses an optimal estimation retrieval approach that provides the information content and the vertical sensitivity (derived from the averaging kernels, for more details see Shephard and Cady-Pereira, 2015), and robust and straightforward retrieval error estimates based on retrieval input parameters. The quality of the retrieval has so far not been thoroughly examined against other observations. Shephard and Cady-Pereira (2015) used Observing System Simulation Experiment (OSSE) studies to evaluate the initial performance of the CrIS NH_3 retrieval, and report a small positive retrieval bias of 6% with a standard deviation of ±20% (ranging from ±12 to ±30% over the vertical profile). Note that no potential systematic errors were included in these OSSE simulations. Their study also shows good qualitative comparisons with the Tropospheric Emission Spectrometer (TES) satellite (Shephard et al., 2011) and the ground-level in situ Quantum Cascade-Laser (QCL) observations (Miller et al., 2014) for a case study over the Central Valley in CA, USA, during the DISCOVER-AQ campaign. However, currently there has not been an extensive validation of the CrIS NH_3 retrievals using direct comparisons against vertical profile observations. In this study we will provide both direct comparisons of the CrIS retrieved profiles against ground-based FTIR observations, and comparisons of CrIS total column values against the FTIR and IASI.

Formatted: Not Superscript/ Subscript

2. Methods

2.1 The CrIS Fast Physical Retrieval

CrIS was launched in late October 2011 on board the Suomi NPP platform. CrIS follows a sun-synchronous orbit with a daytime overpass time at 13:30 local time (ascending) and a night time equator overpass at 1:30. The instrument scans along a 2200 km swath using a 3 x 3 array of circular shaped pixels with a diameter of 14 km at nadir for each pixel, becoming larger ovals away from nadir. In this study we use the NH_3 retrieval as described by Shephard and Cady-Pereira (2015). The retrieval is based on an optimal estimation approach (Rodgers, 2000) that minimizes the differences between CrIS spectral radiances and simulated forward model radiances computed from the Optimal Spectral Sampling (OSS) OSS-CrIS (Moncet et al., 2008), which is built from the well-validated Line-By-Line Radiative Transfer Model (LBLRTM) (Clough et al., 2005; Shephard et al., 2009; Alvarado et al., 2013) and uses the HITRAN database (Rothman et al., 2014) for its spectral lines. The fast computational speed of OSS facilitates the operational production of CrIS retrieved (Level 2) products using an optimal estimation retrieval approach (Moncet et al., 2005). The CrIS OSS radiative transfer forward model computes the spectrum for the full CrIS LW band, at the CrIS spectral resolution of 0.625 cm^{-1} (Tobin, 2012), thus the complete NH_3 spectral band (near 10 μm) is available for the retrievals. However, only a small number of micro windows are selected for the CrIS retrievals to both maximize the information content and minimize the influence of errors. Worden et al., (2004) provides an example of a robust spectral region selection process that takes into consideration both the estimated errors (i.e. instrument noise, spectroscopy errors, interfering species, etc.) and the associated information content in order to select the optimal spectral regions for the retrieval. The a-priori profiles selection for the optimal estimation retrievals follows the Tropospheric Emission Spectrometer (TES) retrieval algorithm (Shephard et al., 2011); Based on the relative NH_3 signal in the spectra the a-priori is selected from one of three possible profiles representing unpolluted, moderate, and polluted conditions. The initial guess profiles are also selected from these three potential profiles.

An advantage of using an optimal estimation retrieval approach is that averaging kernels (sensitivity to the true state) and the estimated errors of the retrieved parameter are computed in a robust and straight-forward manner (for more details see Shephard and Cady-Pereira, 2015). The total satellite retrieved parameter error is expressed as the sum of the smoothing error (due to unresolved fine structure in the profile), the measurement error (random instrument noise in the radiance spectrum propagated to the retrieval parameter), and systematic errors from uncertainties in the non-retrieved forward model parameters and cross-state errors propagated from retrieval-to-retrieval (i.e. major interfering species such as H_2O, CO_2, and O_3) (Worden et al., 2004). As of yet we have not included error estimates for the systematic errors. The CrIS smoothing error is computed, but since in these FTIR comparison results we apply the FTIR observational operator (which accounts for the smoothing error), the smoothing error contribution is not included in the CrIS errors reported in the comparisons. Thus,

Formatted: Subscript

Formatted: Subscript

Formatted: Subscript

only the measurement errors are reported for observations used here; these errors can thus be considered the lower limit on the total estimated CrIS retrieval error.

Figure 1 shows an example of CrIS NH_3 observations surrounding one of the ground-based FTIR instruments. This is a composite map of all days in Bremen with observations in 2015. This figure shows the wide spread elevated amounts of NH_3 across north-western Germany as observed by CrIS.

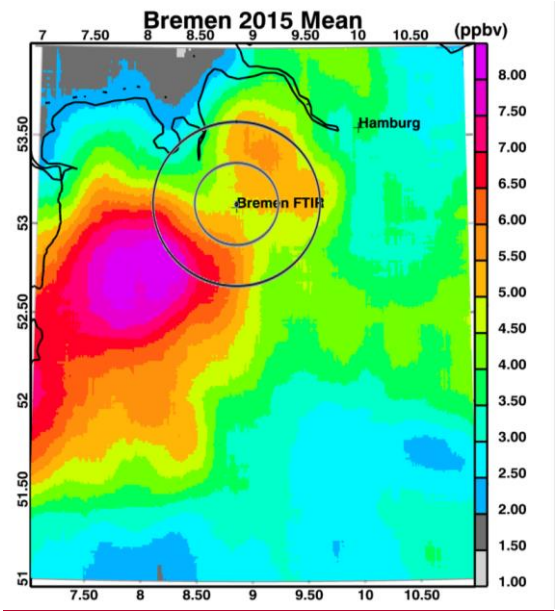

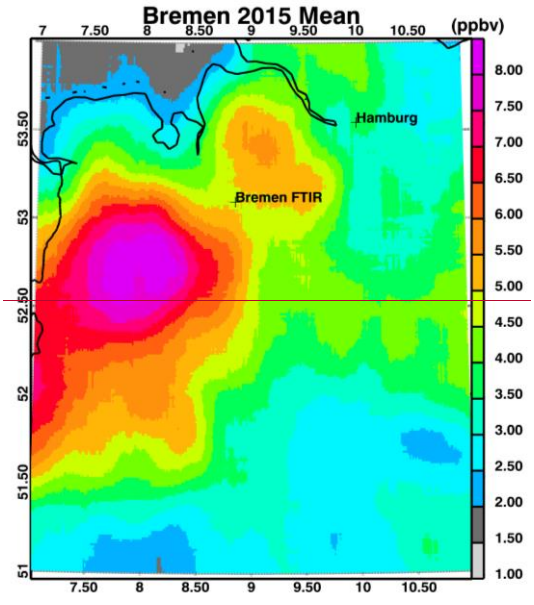

Figure 1. Annual mean of the CrIS retrieved NH_3 surface VMR values around the Bremen FTIR site for 2015. The two circles show the collocation area when for radii of 25 and 50 km.

Since the goal of this analysis is to evaluate the CrIS retrievals that provide information beyond the a-priori, we only performed comparisons when the CrIS spectrum presents a NH_3 signal. We also focused our efforts on

FTIR stations that have FTIR observations with total columns larger than 5 x 10^{15} molecules cm^{-2}(~1-2 ppb surface VMR). This restriction does mean that a number of sites of the FTIR-NH_3 dataset will not be used. For comparability of this study to the results of the IASI-LUT evaluation in an earlier study by Dammers et al., (2016a) we include a short paragraph on the performance of the IASI-LUT and the more recent IASI-NN product when applying similar constraints.

2.2 FTIR-NH_3 retrieval

The FTIR-NH_3 product used in this study is similar to the set described in Dammers et al. (2016a) and is based on the retrieval methodology described by Dammers et al. (2015). The retrieval methodology uses two spectral micro-windows whose spectral width depends on the NH_3 background concentration determined for the observation stations and location (wider window for stations with background concentrations less than one ppb). NH_3 is retrieved by fitting the spectral lines in the two micro-windows MW1 [930.32-931.32 cm^{-1} or wide: 929.40-931.40 cm^{-1}] and MW2 [962.70-970.00 cm^{-1} or wide: 962.10-970.00 cm^{-1}. An optimal estimation approach (Rodgers et al., 2000) is used, implemented in the SFIT4 algorithm (Pougatchev et al., 1995; Hase et al., 2004, 2006). There are a number of species that can interfere to some extent in both windows, with the major species being H_2O, CO_2 and O_3 and the minor species N_2O, HNO_3, CFC-12, and SF_6. The HITRAN 2012 database (Rothman et al., 2014) is used for the spectral lines. A further set of spectroscopic line parameter adjustments are added for CO_2 taken from the ATMOS database (Brown et al., 1996) as well as a set of pseudo-lines for the broad absorptions by the CFC-12 and SF_6 molecules (created by NASA-JPL, G.C. Toon, http://mark4sun.jpl.nasa.gov/pseudo.html). The NH_3 a-priori profiles are based on balloon measurements (Toon et al., 1999) and refitted to match the local surface concentrations (depending on the station either measured or estimated by model results). For the interfering species a-priori profiles we use the Whole Atmosphere Community Climate Model (WACCM, Chang et al., 2008, v3548). The estimated errors in the FTIR-NH_3 retrievals are in the order of ~30% (Dammers et al., 2015) with the uncertainties in the NH_3 line spectroscopy being the most important contributor. Based on the data requirements in section 2.1, a set of seven stations is used (Table 1). For all sites except Wollongong in Australia we use the basic narrow spectral windows. For Wollongong the wide spectral windows are used. For a more detailed description of each of the stations see the publications listed in Table 1 or Dammers et al. (2016a).

Table 1. The location, longitudinal and latitudinal position, altitude above sea level, and type of instrument for each of the FTIR sites used in this study. In addition, a reference is given to a detailed site description, when available.

Station	Lon (degrees)	Lat (degrees)	Altitude (m.a.s.l)	FTIR instrument	Reference
Bremen, Germany	8.85E	53.10N	27	Bruker 125 HR	Velazco et al., 2007
Toronto, Canada	79.60W	43.66N	174	ABB Bomem DA8	Wiacek et al., 2007 Lutsch et al., 2016
Boulder, United States	105.26W	39.99N	1634	Bruker 120 HR	
Pasadena, United States	118.17W	34.20N	350	MkIV_JPL	
Mexico City, Mexico	99.18W	19.33N	2260	Bruker Vertex 80	Bezanilla et al., 2014
Wollongong, Australia	150.88E	34.41S	30	Bruker 125 HR	
Lauder, New Zealand	169.68E	45.04S	370	Bruker 120 HR	Morgenstern et al., 2012

2.3 IASI-NH_3

The CrIS retrieval will also be compared with corresponding IASI/FTIR retrievals using results from a previous study by Dammers et al. (2016a). Both the IASI-LUT (Van Damme et al., 2014a) and the IASI-NN (Neural Networks, Whitburn et al., 2016) retrievals from observations by the IASI instrument aboard MetOp-A will be used. A short description of both IASI retrievals is provided here, for a more in-depth description, see the respective publications by Van Damme et al. (2014a) and Whitburn et al. (2016). The IASI instrument on board the MetOp-A platform is in a sun-synchronous orbit and has a daytime overpass at around 9:30 local solar time and a night time overpass at around 21:30. The instrument has a circular footprint of about 12 km diameter for nadir viewing angles with of nadir observations along a swath of 2100 km. Both IASI retrievals are based on the calculation of a dimensionless spectral index called the Hyperspectral Range Index (HRI) (Van Damme et al., 2014a). The HRI is representative of the amount of NH_3 in the measured column. The IASI-LUT retrieval makes a direct conversion of the HRI to a total column density with the use of a look-up-table (LUT). The LUT is created using a large number of simulations for a wide range of atmospheric conditions which links the Thermal Contrast (TC, the difference between the air temperature at 1.5 km altitude and the temperature of the Earth surface) and the HRI to a NH_3 total column density. The retrieval includes a retrieval error based on the uncertainties in the initial HRI and TC parameters. The more recent IASI-NN retrieval (Whitburn et al., 2016) follows similar steps but it makes use of a neural network. The neural network combines the complete temperature, humidity and pressure profiles for a better representation of the state of the atmosphere. At the same time the retrieval error estimate is improved by including error terms for the uncertainty in the profile shape, and the full temperature and water vapour profiles. The IASI-NN version uses the fixed profiles that were described by Van Damme et al., (2014) but allows for the use of third party profiles to improve the representation of the NH_3 atmospheric profile. The IASI-LUT and IASI-NN retrievals have both been previously compared with FTIR observations (Dammers et al., 2016a, Dammers et al., 2016b). They compared reasonably well with correlations around r=0.8 for a set of FTIR stations, with an underestimation of around 30% that depends slightly on the magnitude of total column amounts, with the IASI-NN performing slightly better.

2.4 Data criteria & quality

NH_3 concentrations show large variations both in space and time as the result of the large heterogeneity in emission strengths due to spatially variable sources and drivers such as meteorology and land use (Sutton et al., 2013). This high variability poses challenges in matching ground-based point observations made by FTIR observations with CrIS downward-looking satellite measurements which have a 14-km nadir footprint. For the pairing of the measurement data we apply data selection criteria similar to that described in Dammers et al. (2016a) and summarized in Table 2. To minimize the impact of the heterogeneity of the sources, we choose a maximum of 50 km between the centre points of the CrIS observations and the FTIR site location. To diminish the effect of temporal differences between the FTIR and CrIS observations a maximum time difference of 90 minutes is used. Topographical effects are reduced by choosing a maximum altitude difference of 300 m at any point between the FTIR site location and the centre point of the satellite pixel location. The altitude differences are calculated using the Space Shuttle Radar Topography Mission Global product at 3 arc-second resolution (SRTMGL3, Farr et al., 2007). To ensure the data quality of CrIS-NH_3 retrieval for Version 1.0, a small number of outliers with a maximum retrieved concentration above 200 ppb (at any point in the profile) were removed

from the comparison dataset. While potentially a surface NH_3 value of 200 ppb (and above) would be possible (i.e. downwind of forest fires), it is highly unlikely to occur over the entire footprint of the satellite instrument. Moreover, after inspecting these data points, they seem to be affected by numerical issues in the fitting procedure (possibly due to interfering species). As we are interested in validating the CrIS observational information (not just a-priori information), we only select comparisons that contain some information from the satellite (degrees of freedom for signal (DOFS) ≥ 0.1). Do note that on average the observations have a DOFS between 0.9 and 1.1. The DOFS > 0.1 filter only removes some of the outliers at the lower end. No explicit filter is applied to account for clouds; however, clouds will implicitly be accounted for by the quality control as CrIS will not measure a NH_3 signal (e.g. DOFS < 0.1) below optically thick clouds (e.g. cloud optical depth >~1). In addition, the CrIS observations are matched with FTIR observations taken only during clear-sky conditions, which mostly eliminates influence from cloud cover. Finally, the high signal to noise ratios (SNR) of the CrIS instrument, allows it to retrieve NH_3 from a thermal contrast approaching 0 K during daytime observations (Clarisse et al., 2010). Given this, we decided not to apply a thermal contrast filter to the CrIS data. No additional filters are applied to the FTIR observations beyond the clear-sky requirement.

For both IASI retrievals, we use the same observation selection criteria as described in Dammers et al. (2016a). The set of criteria is similar to those used here for the CrIS observations. Observations from both IASI retrievals are matched using the overpass time, and longitudinal and latitudinal positions. For comparability with CrIS a spatial difference limit of 50 km limit was used, instead of the 25 km spatial limit used in the previous study. Furthermore we apply the thermal contrast (> 12K, difference between the temperatures at 1.5 km and the surface) and Earth skin temperature criteria to the IASI observations to match the previous study.

Table 2. Coincidence criteria and quality flags applied to the satellite and FTIR data. The third through fifth columns show the number of observations remaining after each subsequent data criteria step and the number of possible combinations between the CrIS and FTIR observations. The first set of numbers indicate the number of CrIS observations within a 1°x 1° degree square surrounding the FTIR site.

Filter	**Data Criteria**	**Nr. Obs.**		
		FTIR	**CrIS**	**Combinations**
CrIS		15661	25855	
Temporal sampling difference	Max 90 min	1576	13959	112179
Spatial sampling difference	Max 50 km	1514	3134	22869
Elevation difference	Max 300 m	1505	1642	9713
Quality flag	DOFS ≥ 0.1	1433	1453	8579

2.5 Observational Operator Application

To account for the vertical sensitivity and the influence of the a-priori profiles of both retrievals we apply the observational operator (averaging kernel and a-priori of the retrieval) of the FTIR retrieval to the CrIS retrieved profiles. The CrIS observations are matched to each individual FTIR observation in time and space following the matching criteria. The FTIR averaging kernels, a-priori profiles, and retrieved profiles are first mapped to the CrIS pressure levels (fixed pressure grid, layers are made smaller or cut off for observations above elevation

to fit the fixed pressure grid). Following Rodgers and Connor (2003) and Calisesi et al. (2005) this results in the mapped FTIR averaging kernel, $\boldsymbol{A}_{ftir}^{mapped}$, the mapped FTIR apriori, $\boldsymbol{x}_{ftir}^{mapped,apriori}$, and the mapped FTIR retrieved profile, $\boldsymbol{x}_{ftir}^{mapped}$. Then we apply the FTIR observational operator to the CrIS observations using **eq. (1)**.

$$\hat{\boldsymbol{x}}_{CrIS} = \boldsymbol{x}_{ftir}^{mapped,apriori} + \boldsymbol{A}_{ftir}^{mapped}(\boldsymbol{x}_{CrIS} - \boldsymbol{x}_{ftir}^{mapped,apriori}) \quad \textbf{(1)}$$

$$\widehat{\Delta \boldsymbol{x}}_{abs} = \hat{\boldsymbol{x}}_{CrIS} - \boldsymbol{x}_{ftir}^{mapped} \quad \textbf{(2)}$$

$$\widehat{\Delta \boldsymbol{x}}_{rel} = (\hat{\boldsymbol{x}}_{CrIS} - \boldsymbol{x}_{ftir}^{mapped})/(\mathbf{0.5}\ \boldsymbol{x}_{ftir}^{mapped} + \mathbf{0.5}\ \hat{\boldsymbol{x}}_{CrIS}) \quad \textbf{(3)}$$

where $\boldsymbol{x}_{ftir}^{apriori}$ is the FTIR a-priori profile, $\boldsymbol{x}_{ftir}^{mapped}$ is the interpolated FTIR profile, $\boldsymbol{A}_{ftir}^{mapped}$is the FTIR averaging kernel, and $\hat{\boldsymbol{x}}_{CrIS}$ is the smoothed CrIS profile.

The CrIS smoothed profile $\hat{\boldsymbol{x}}_{CrIS}$ calculated from equation (1) provides an estimate of the FTIR retrieval applied to the CrIS satellite profile. Next we evaluate both total column and profile measurements.

For the first validation step, following Dammers et al. (2016a), who evaluated the IASI-LUT (Van Damme et al., 2014a) product, we sum the individual profile ($\hat{\boldsymbol{x}}_{CrIS}$) to obtain a column total to compare to the FTIR total columns. This step gives the opportunity to evaluate the CrIS retrieval in a similar manner as was done with the IASI-LUT retrieval. If multiple FTIR observations match a single CrIS overpass we also average those together into a single value as well as each matching averaged CrIS observation. Therefore, it is possible to have multiple FTIR observations, each with multiple CrIS observations all averaged into a single matching representative observation. For the profile comparison this averaging is not performed to keep as much detail available as possible. An important point to make is that this approach assumes that the FTIR retrieval gives a better representation of the truth. While this may be true, the FTIR retrieval will not match the truth completely. For readability we assume that the FTIR retrieval indeed gives a better representation of the truth, and in the next sections will describe the case in which we apply the FTIR observational operator to the CrIS values. For the tenacious reader we included a similar set of results in the appendix, using the CrIS observational operator instead of the FTIR observational operator, as the assumption of the FTIR being truth is not exactly right.

3. Results and discussion

3.1 Total column comparison

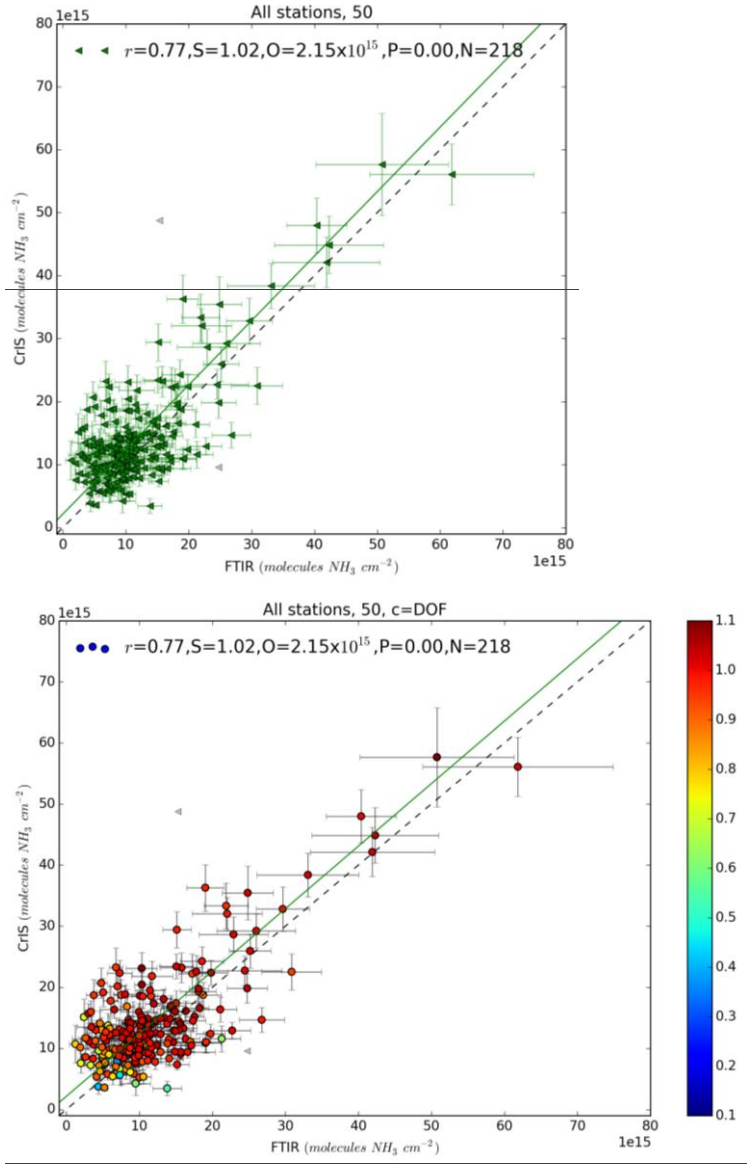

Figure 2. Correlation between the FTIR and CrIS total columns using the coincident data from all measurement sites. The horizontal and vertical bars show the total estimated error on each FTIR and CrIS observation. The colouring on the scatter indicates the mean DOF of each the CrIS coincident data. The trend line shows the results of the regression analysis.

The total columns are averaged as explained in Section 2.4 to show a direct comparison of FTIR measurements with CrIS observations in Figure 2. A three sigma outlier filter was applied to calculate the regression statistics. The filtered outliers are displayed in grey, and may be caused by low information content (DOFS) and terrain characteristics. For the regression we used the reduced major axis regression (Bevington and Robinson, 1992), accounting for possible errors both in the x and y values. There is an overall agreement ~~is good~~ with a correlation of r = 0.77 (P < 0.01, N = 218) and a slope of 1.02 (+- 0.05). At the lower range of values the CrIS column totals are ~~significantly~~ higher than the observed FTIR values. Possibly the CrIS retrieval overestimates due to the low sensitivity to low concentrations. Without the sensitivity the retrieval will find a value more closely to the a-priori, which may be too high. Figure 3 shows the comparisons at each station. When the comparisons are broken down by station (Figure 3), the correlation varies from site to site, from a minimum of 0.28 in Mexico City (possibly due to retrieval errors associated with the highly irregular terrain) to a maximum of 0.84 in Bremen. Similarly to Mexico City the comparison also shows an increase in scatter for Pasadena, where the FTIR site is also located on a hill. In Toronto~~,~~ and Bremen ~~and Pasadena~~ there is good agreement when NH_3 is elevated (> 20 x 10^{15} molecules cm^{-2}) ~~in~~, and low bias in the CrIS total columns for intermediate values (between 10 and 20 x 10^{15} molecules cm^{-2}) except for the outlying observation in Bremen, which is marked as an outlier by our three sigma filter used for Figure 2. In Wollongong, there is less agreement between the instruments. There are two comparisons with large CrIS to FTIR ratios while most of the other comparisons also show a bias for CrIS. For both cases the bias can be explained by the heterogeneity of the ammonia concentrations in the surrounding regions. The two outlying observations were made during the end of November, 2012, which coincides with wild fires in the surrounding region. Furthermore the Wollongong site is located coastally, which will increase the occurrences where one instrument observes clean air from the ocean while the other observes inland air masses.~~.~~

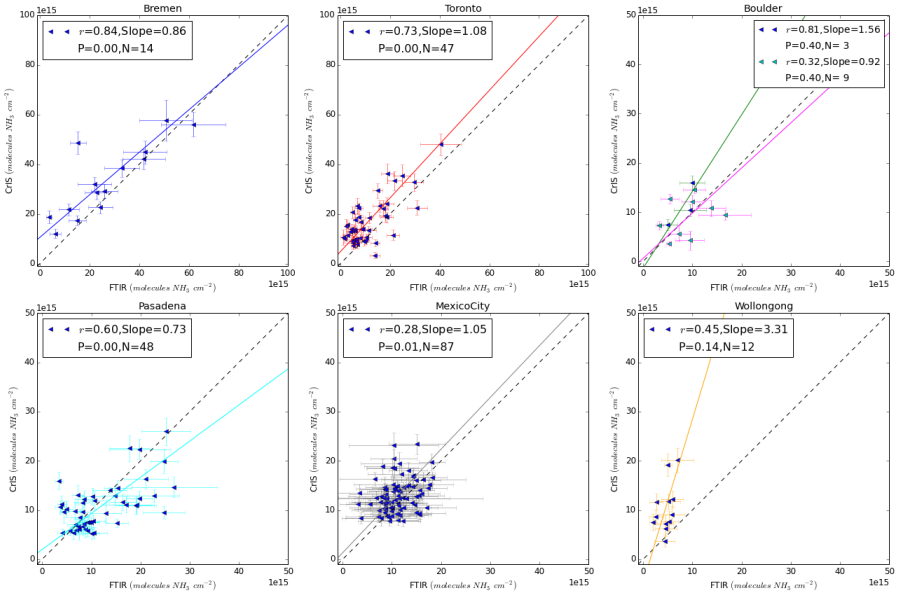

Figure 3. FTIR vs CrIS comparison scatter plots showing the correlations for each of the individual stations, with estimates error plotted for each value. The trend lines show the individual regression results. Note the different ranges on the x and y axis. The results for the Boulder (green line) and Lauder (pink line) sites are shown in the same panel.

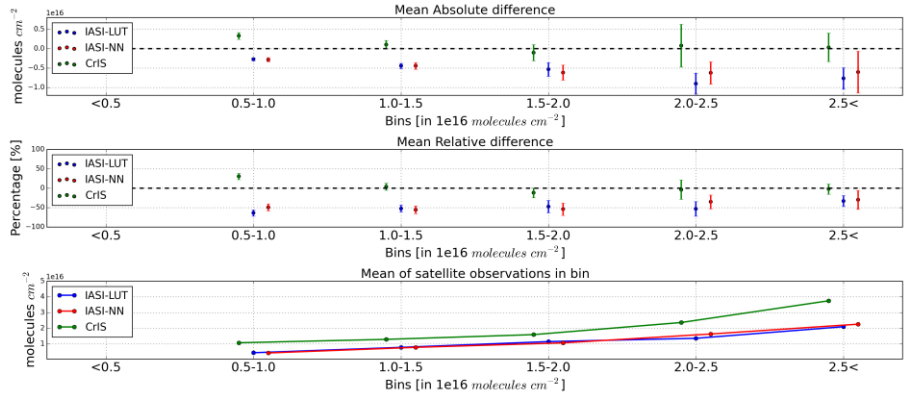

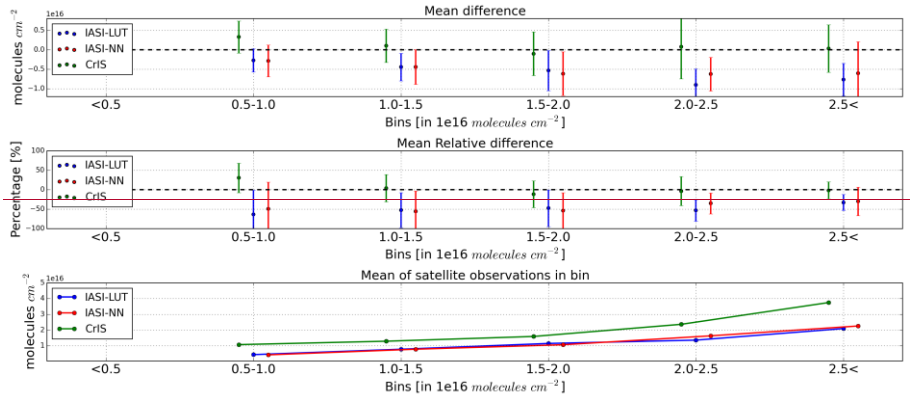

Figure 4. Plots of the mean absolute and relative differences between CrIS and IASI, as a function of NH_3 total column. Observations are separated into bins of total columns. The upper panel shows the mean absolute difference (MD). The middle panel shows the mean relative difference. The bars in these top two panels show the ~~standard deviation~~95 % confidence interval for each value. The bottom panel shows the mean of the observations in each bin. The number of observations in each set is shown in the bottom panel.

The mean absolute (MD) and relative difference (MRD) are calculated following equation 4 and equation 5;

$$MRD = \frac{1}{N}\sum_{i=1}^{N}\frac{(CrIS\ column_i - FTIR\ column_i)\ x\ 100}{0.5*FTIR\ column_i + 0.5*CrIS\ column_i} \quad \textbf{(4)}$$

$$MD = \frac{1}{N}\sum_{i=1}^{N}(CrIS\ column_i - FTIR\ column_i) \quad \textbf{(5)}$$

with N being the number of observations.

Table 3. Results of the total column comparisons of the FTIR to CrIS, FTIR to IASI-LUT and FTIR to IASI-NN. N is the number of averaged total columns, MD is the mean difference [10^{15} molecules cm^{-2}], MRD is the mean relative difference [frac, in %]. Take note that the combined value N does not add up with all the separate sites as observations have been included for FTIR total columns > 5 x 10^{15} molecules cm^{-2}.

Retrieval	Column total range in molecules cm^{-2}	N	MD in 10^{15} (1σ)	MRD in % (1σ)	FTIR mean in 10^{15} (1σ)
CrIS-NH3	< 10.0 x 10^{15}	93	3.3 (4.1)	30.2 (38.0)	7.5 (1.5)
CrIS-NH3	>= 10.0 x 10^{15}	109	0.4 (5.3)	-1.39 (34.4)	16.7 (8.5)
IASI-LUT	< 10.0 x 10^{15}	229	-2.7 (3.0)	-63.6 (62.6)	7.1 (1.4)
IASI-LUT	>= 10.0 x 10^{15}	156	-5.1 (4.2)	-50.2 (43.6)	14.8 (6.7)
IASI-NN	< 10.0 x 10^{15}	212	-2.2 (3.6)	-57.0 (68.7)	7.1 (1.4)
IASI-NN	>= 10.0 x 10^{15}	156	-5.0 (5.1)	-52.5 (49.7)	14.8 (6.7)

We evaluate the data by subdividing the comparisons over a set of total column bins as a function of the FTIR total column value of each individual observation. The bins (with a range of 5 x10^{15} to 25 x10^{15} molecules cm^{-2} with iterations steps of 5 x 10^{15} molecules cm^{-2}) give a better representation of the performance of the retrieval as it shows the influence of the retrieval as a function of magnitude of the total column densities. The results of these total column comparisons are presented in Figure 4. Table 3 summarizes the results for each of the FTIR to satellite column comparisons into two total column bins, which splits the comparisons between smaller and larger than 10 x 10^{15} molecules cm^{-2}. A few combinations of the IASI-NN and FTIR retrievals have a small denominator value that causes problems in the calculation of the MRD. A three sigma outlier filter based on the relative difference is applied to remove these outliers (<10 x 10^{15} molecules cm^{-2}, only the IASI-NN set). The statistical values are not given separately by site because of the low number of matching observations for a number of the sites.

The CrIS/FTIR comparison results show a large positive difference in both the absolute (MD) and relative (MRD) for the smallest bin, (5.0-10.0 x 10^{15} molecules cm^{-2}). The rest of the CrIS/FTIR comparison bins with NH_3 values > 10.0 x 10^{15} agree very well with a nearly constant bias (MD) around zero, and a standard deviation of the order of 5.0 x 10^{15} that slightly dips below zero in the middle bin. The standard deviation over these bins is also more or less constant, and the weak dependence on the number of observations in each bin indicates that most of the effect is coming from the random error on the observations. The relative difference becomes systematically smaller with increasing column total amounts, and tend towards zero with a standard deviation ~25-50%, which is on the order of the reported estimated errors of the FTIR retrieval (Dammers et al, 2015).

For a comparison against previous reported satellite results, we included both the IASI-LUT (Van Damme et al., 2014a) and the IASI-NN (Whitburn et al., 2016) comparisons against the FTIR observations. To put the results of this study into perspective of the IASI-LUT and IASI-NN products we added Figure A1 to the Appendix, which shows the total column comparison for both products. Both IASI products show similar differences as a function of NH_3 column bins, which is somewhat different from the CrIS/FTIR comparison results. The absolute difference (MD) is mostly negative with the smallest factor for the smallest total column bin, with a difference around -2.5 x 10^{15} (std = ±3.0 x 10^{15}, N = 229) molecules cm^{-2} that slowly increases as a function of the total

column. However, the relative difference (MRD) is at its maximum for the smaller bin with a difference of the order -50% (std = ±~50%, N=229) which decreases to ~ -10-25% (std = ±25%) with increasing bin value. For both the IASI-NN and IASI-LUT retrievals we find an underestimation of the total columns, which originates mostly from a large systematic error in combination with more randomly distributed error sources such as the instrument noise and interfering species, which is similar to results reported earlier for IASI-LUT (Dammers et al., 2016b).

A number of factors, besides the earlier reported FTIR uncertainties, can explain the differences between the FTIR and CrIS measurements. The small positive bias found for CrIS points to a small systematic error. The higher SNR, from both the low radiometric noise and high spectral resolution, ~~along with the shorter atmospheric path lengths for observations from the ground-based solar-pointing FTIR instrument,~~ enables it to resolve smaller gradients in the retrieved spectra, which potentially can provide greater vertical information and detect smaller column amounts (lower detection limit). This could explain the larger MRD and MD CrIS differences at the lower end of the total column range. However, a number of standalone tests with the FTIR retrieval showed only a minor increase in the total column following a decrease in spectral resolution, which indicates that the spectral resolution itself is not enough to explain the difference.

3.2 Profile Comparison

The CrIS satellite and FTIR retrieved profiles are matched using the criteria specified above in Table 2 and compared. It is possible for a CrIS observation to be included multiple times in the comparison as there can be more than one FTIR observation per day, and /or, the possibility of multiple satellite overpasses that match a single FTIR observation.

A representative profile example

An example of the profile information contained in a representative CrIS and FTIR profile is shown in Fig. 5. Although the vertical sensitivity and distribution of NH_3 differs per station this is a fairly representative. The FTIR usually has a somewhat larger DOFS in the order of 1.0-2.0, mostly depending on the concentration of NH_3, compared to the CrIS total of ~1 DOFS. Figure 5a shows an unsmoothed FTIR averaging kernel [vmr vmr^{-1}] of a typical FTIR observation. The averaging kernel (AVK) peaks between the surface and ~850 hPa, which is typical for most observations. In specific cases with plumes overpassing the site, the averaging kernel peak is at a higher altitude matching the location of the NH_3 plume. The CrIS averaging kernel (Fig. 5b) usually has a maximum somewhere in between 680-850 hPa depending on the local conditions. This particular observation has a maximum near the surface, an indication of a day with ~~good~~ high thermal contrast. Both the FTIR and CrIS concentration profiles have a maximum at the surface with a continuous decrease that mostly matches the a-priori profile in shape following the low DOFS. This is visible for layers at the lower pressures (higher altitudes) where the FTIR and CrIS a-priori and retrieved volume mixing ratios become similar and near zero. The absolute difference between the FTIR and CrIS profiles can be calculated by applying the FTIR observational operator to the CrIS profile, as we described in section 2.5. The largest absolute difference (Fig. 5d) is found at the surface, which is also generally where the largest absolute NH_3 values occur. The FTIR smoothed relative difference (red, striped line) peaks at the pressure where the sensitivity of the CrIS retrieval is highest (~55%), which goes down to ~20-30% for the higher altitude and surface pressure layers. Overall the

retrievals agree ~~well~~ with most of the difference explained by the estimated errors of the individual retrievals. For an illustration of the systematic and random errors on the FTIR and CrIS profiles shown in Fig 5, see the figures in the appendix: for the FTIR error profile see Fig. A2~~1~~ (absolute error) and A3~~2~~ (relative error) and for the CrIS measurement error profile see Fig. A4~~3~~. Please note that we only show the diagonal error covariance values for each of the errors, which is common practice. The total column of our example profile is ~20 x 10^{15} molecules cm^{-2} which is a slightly larger value than average. The total random error is < 10% for each of the layers, mostly dominated by the measurement error, which is somewhat smaller than average (Dammers et al., 2015) following the larger NH_3 VMR. A similar value is found for the CrIS measurement error with most layers showing an error < 10%. The FTIR systematic error is around ~10% near the surface and grows to a larger 40% for the layers between 900 – 750 hPa. The error is mostly due to the errors in the NH_3 spectroscopy (Dammers et al., 2015). The shape of the relative difference between the FTIR and CrIS closely follows the shape systematic error on the FTIR profile pointing to that error as the main cause of difference.

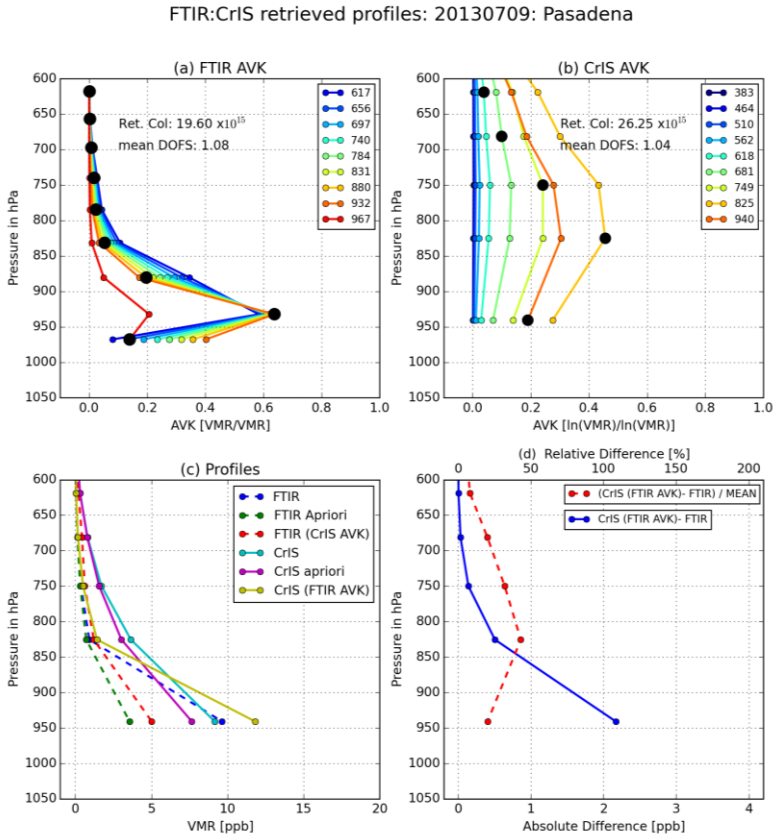

Figure 5. Example of the NH_3 profile comparison for an FTIR profile matched with a CrIS profile measured around the Pasadena site. With (a) the FTIR averaging kernel, (b) the CrIS averaging kernel. For both averaging kernels the black dots show the matrices diagonal values. Panel (c) shows the retrieved profiles of both FTIR

(blue) and CrIS (cyan) with the FTIR values mapped to the CrIS pressure layers. Also shown are the FTIR a-priori (green), the CrIS a-priori (purple), the CrIS retrieved profile smoothed with the FTIR averaging kernel [CrIS (FTIR AVK)] (yellow) and the FTIR profile smoothed with the CrIS averaging kernel [FTIR (CrIS AVK)](red). In panel (d), the blue line is the absolute difference between the FTIR profile (blue, panel (c)) and the CrIS profile smoothed with the FTIR averaging kernel (Yellow, panel (c)) with the red line the corresponding relative difference.

All paired data

In Fig. 6 all the individual site comparisons were merged. The Mexico City site was left out of this figure because of the large number of observations in combination with a difference in pressure grid due to the high altitude of the city ~~which~~ obscured the overall analysis and biased the results towards the results of one station. Similar to the single profile example, the FTIR profile peaks near the surface for most observations, slowly going towards zero with decreasing pressure. Compared to the representative profile example a number of differences emerge. A number of FTIR observations peak further above the surface and are shown as outliers, which drag the mean further away from the median values. The combined CrIS profile in Fig. 6 shows a similar behaviour, although for the lowest pressure layer it has a lower median and mean compared to the layer above. The difference between Fig. 5 and Fig. 6e derives mostly from the number of observations used in the boxplot, many with weak sensitivity at the surface. Similar to the single profile example in Fig. 5, the FTIR averaging kernels in Fig. 6c on average peak near or just above the surface (with the diagonal elements of the AVK's shown in the figure). The sensitivity varies a great deal between the observations as shown by the large spread of the individual layers. The CrIS averaging kernels (Fig. 6g) usually peak in the boundary layer around the 779 hPa layer with the 2 surrounding layers having somewhat similar values. The instrument is less sensitive to the surface layer as is demonstrated by the large decrease in the AVK near the surface, but this varies depending on the local conditions. We find the largest absolute differences in the lower three layers, as was seen in the example in Fig. 5, although the differences decrease downwards rather than increase. The relative difference shows a similar shape to Fig 5. Overall both retrievals ~~agree quite well~~show agreement. The relative differences in the single level retrieved profile values in Fig. 6h show an average difference in the range of ~20 to 40% with the 25th and 75th percentiles at around 60-80%, which partially follows from our large range of concentrations. The absolute difference shows an average difference in the range of -0.66 to 0.87 ppb around the peak sensitivity levels of the CrIS observations (681 to 849 hPa). The lower number of surface observations follow from the fact that only the Bremen site is located at an altitude low enough for the CrIS retrieval to provide a result at this pressure level~~.~~. ~~Because of~~Due to this difference in retrieval layering, the remaining 227 observations mostly follow from matching observations in Bremen, which is located in a region of significant NH_3 emissions.

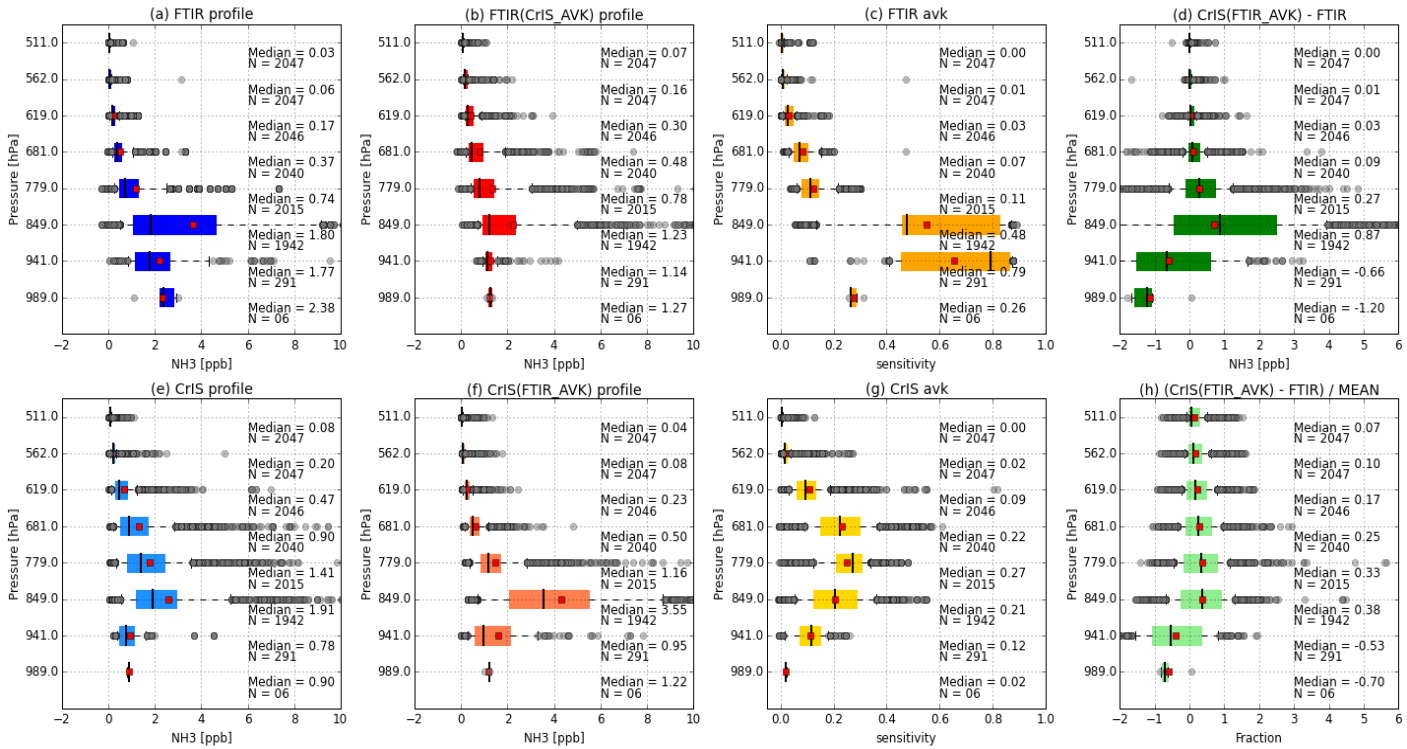

Figure 6. Profile comparison for all stations combined. Observations are combined following pressure "bins", i.e. the midpoints of the CrIS pressure grid. Subplot (a) shows the mean profiles of the FTIR (blue), (b) the profiles of FTIR with the CrIS averaging kernel applied to it (red), (c) the FTIR averaging kernel diagonal values, and (d) shows the absolute difference [VMR] between profiles (f) and (a). The second row shows the CrIS mean profile in (e), (f) the profiles of CrIS with the FTIR averaging kernel applied, (g) the CrIS averaging kernel diagonal values, (h) the relative difference [Fraction] between the profiles in (f) and (a). Each of the boxes edges are the 25th and 75th percentiles, the black lines in each box is the median, the red ~~diamond~~ square is the mean, the whiskers are the 10th and 90th percentiles, and the grey circles are the outlier values outside the whiskers.

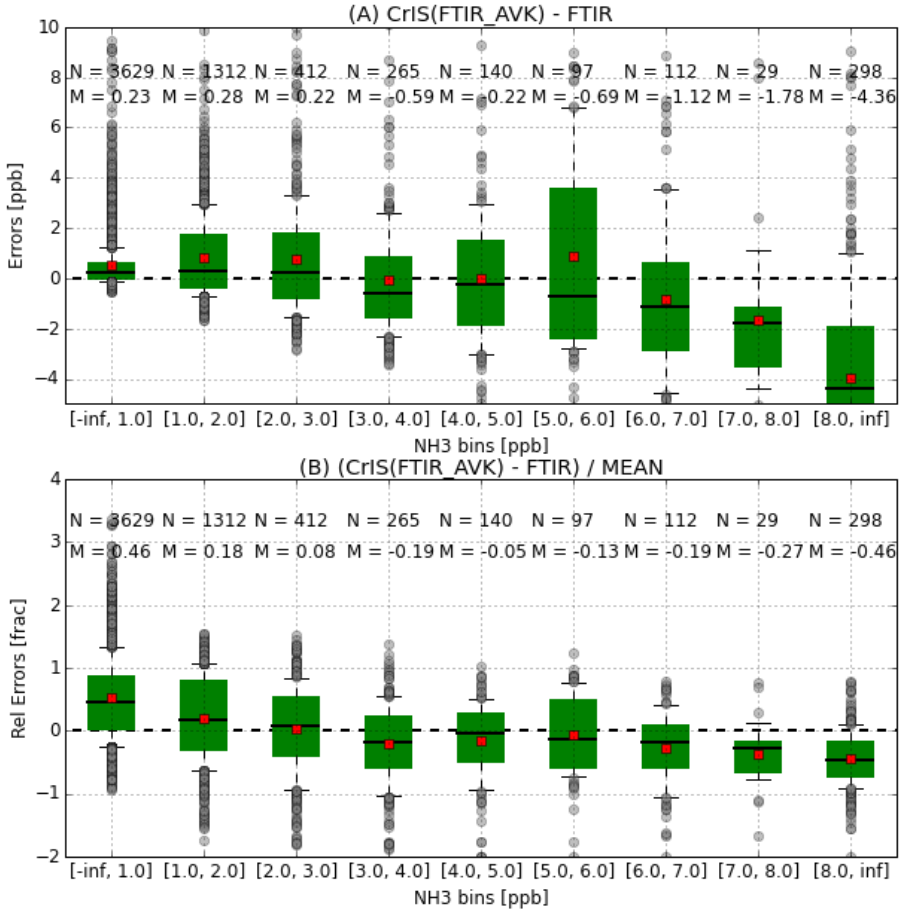

Figure 7. Summary of the ~~errors~~ absolute and relative actual error as a function of the VMR of NH_3 in the individual FTIR layers. The box edges are the 25th and 75th percentiles, the black line in the box is the median, the red square ~~diamond~~ is the mean, the whiskers are the 10th and 90th percentiles, and the grey circles are the outlier values outside the whiskers. Only observations with a pressure greater than 650 hPa are used. The top panel shows the absolute difference for each VMR bin, the bottom panel shows the relative difference for each VMR bin.

The switch between negative and positive values in the absolute difference (see Fig. 6d), occurs in the two lowest layers dominated by the Bremen observations and provides insight into the relation between absolute differences as function of retrieved concentration. Fig. 7 shows a summary of the differences as a function of the individual NH_3 VMR layer amounts. As seen before in the column comparison, e.g. Fig 2 and 4, the CrIS retrieval gives larger total columns than the FTIR retrieval for the small values of VMR. For increasing VMRs, this slowly tends to a negative absolute difference with a relative difference in the range of 20-30%. However,

note that the number of compared values in these high VMR bins are by far lower than in the first three bins leading to relatively less effect in the total column and merged VMR figures (Figs. 2 and 6) from these high VMR bins. We now combine the results of Figs. 6 and 7 into Figure 8 to create a set of subplots showing the difference between both retrieved profiles as a function of the maximum VMR of each retrieved FTIR profile. For the layers with pressure less than 681 hPa we generally find ~~good~~ agreement, which is expected but not very meaningful, since there is not much NH_3 (and thus sensitivity) in these layers and any differences are smoothed out by the application of the observational operator. The relative differences for these layers all lie around ~0-20%. For the lowest two VMR bins we find again that CrIS gives larger results than the FTIR, around the CrIS sensitivity peak in the layer centred around 849 hPa, and to a lesser extent in the layer below. At these VMR levels (< 2 ppb) the NH_3 signal approaches the spectral noise of the CrIS measurement, making the retrievals more uncertain. The switch lies around 2-3 ppb where the difference in the SNR between the instruments becomes less of an issue. Also easily observed is the relation between the concentration and the absolute and relative differences. This can be explained by the difference in sensitivity of the instruments, and the measurement noise of both instruments. For the largest VMR bin [> 4.0 ppb] we find that CrIS is biased for the four lowest layers. Differences are largest in the surface layer where only a few observations are available, almost all from the Bremen site. Most of these CrIS observations have a peak satellite sensitivity at a higher altitude than the FTIR. Assuming that most of the NH_3 can be found directly near the surface, with the concentration dropping off with a sharp gradient as a function of altitude, it is likely that these concentrations are not directly observed by the satellite but are observed by the FTIR instruments. This difference in sensitivity should be at least partially removed by the application of the observational operator but not completely, due to the intrinsic differences between both retrievals. The CrIS retrieval uses one of three available a-priori profiles, which is chosen following a selection based on the strength of NH_3 signature in the spectra. The three a-priori profiles (unpolluted, moderately polluted and polluted) are different in both shape and concentrations. Out of the entire set of 2047 combinations used in Fig. 8, only six are of the not polluted a priori category. About 1/3 of the remaining observations use the polluted a-priori, which has a sharper peak near the surface (see Fig. 5c), compared to the moderately polluted profile, which is used by 2/3s of the CrIS retrievals shown in this work. Based on the results as a function of retrieved VMR (as measured with the FTIR so not a perfect restriction), it is possible that the sharper peak at the surface as well as the low a-priori concentrations are restricting the retrieval. The dependence of the differences on VMR can also possibly follow from uncertainties in the line spectroscopy. In the lower troposphere there is a large gradient in pressure and temperature and the impact of any uncertainty in the line spectroscopy is greatly enhanced. Even for a day with large thermal contrast and NH_3 concentrations (e.g. Fig 5.), the difference between both the CrIS and FTIR retrievals was dominated by the line spectroscopy. This effect is further enhanced by the higher spectral resolution and reduced instrument noise of the FTIR instrument, which potentially makes it more able to resolve the line shapes.

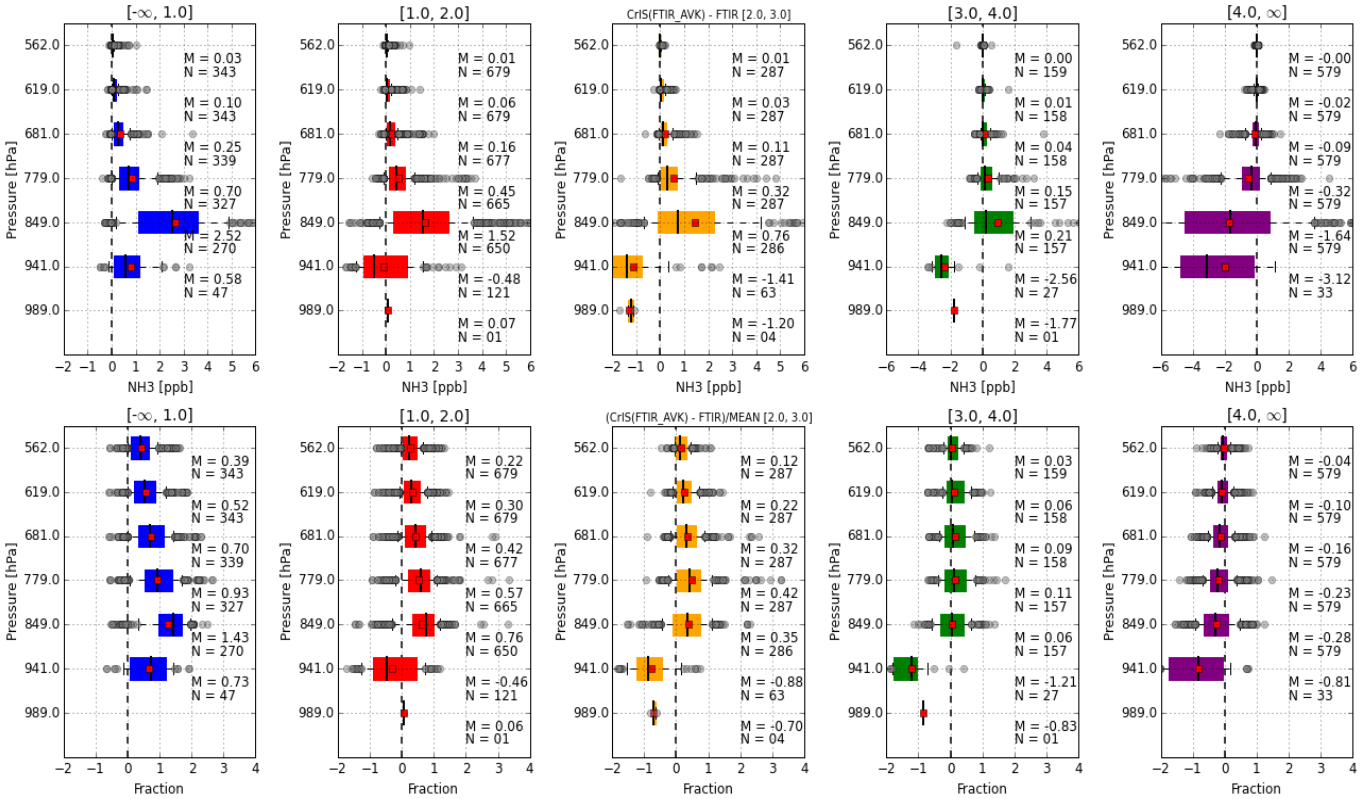

Figure 8. Summary of differences as a function of maximum volume mixing ratio (VMR). The maximum VMR of each FTIR profiles is used for the classification. Absolute (Top row) and relative profile differences (bottom row) following the FTIR and CrIS (FTIR AVK applied) profiles. Observations are following pressure layers, i.e. the midpoints of the CrIS pressure grid. The box edges are the 25th and 75th percentiles, the black line in the box is the median, the red square ~~diamond~~ is the mean, the whiskers are the 10th and 90th percentiles, and the grey circles are the outlier values outside the whiskers.

To summarise, the overall differences between both retrievals are quite small, except for the lowest layers in the NH_3 profile where CrIS has less sensitivity. The differences mostly follow the errors as estimated by the FTIR retrieval and further effort should focus on the estimated errors and uncertainties. A way to improve the validation would be to add a third set of measurements with a better capability to vertically resolve NH_3 concentrations from the surface up to ~750 hPa (i.e. the first 2500 m). One way to do this properly is probably by using airplane observations that could measure a spiral around the FTIR path coinciding with a CrIS overpass. The addition of the third set of observations would improve our capabilities to validate the satellite and FTIR retrievals and point out which retrieval specifically is causing the absolute and relative differences at each of the altitudes.

4. Conclusions

Here we presented the first validation of the CrIS-NH_3 product using ground-based FTIR-NH_3 observations. The total column comparison shows that both retrievals ~~agree well with~~have a correlation of R = 0.77 (P < 0.01, N = 218) and almost no bias with an overall slope of 1.02 (std = ±0.05). For the individual stations we find varying levels of agreement mostly limited by the small range of NH_3 total columns. For FTIR total columns > 10 x 10^{15} molecules cm^{-2} the CrIS and FTIR observations ~~agree very well~~are in agreement with only a small bias of 0.4 (std = ± 5.3) x 10^{15} molecules cm^{-2}, and a relative difference 4.57 (std = ± 35.8) %. In the smaller total column range the CrIS retrieval shows a positive bias with larger relative differences 49.0 (std = ± 62.6) % that mostly seems to follow from observations near the CrIS detection limit. The results of the comparison between the FTIR and the IASI-NN and IASI-LUT retrievals, are comparable to those found in earlier studies. Both IASI products showed smaller total column values compared to the FTIR, with a MRD ~-35- -40%. On average, the CrIS retrieval has one piece of information, while the FTIR retrieval shows a bit more vertical information with DOFS in the range of 1-2. The NH_3 profile comparison shows similar results, with a small mean negative difference between the CrIS and FTIR profiles for the surface layer and a positive difference for the layers above the surface layer. The relative and absolute differences in the retrieved profiles can be explained by the estimated errors of the individual retrievals. Two causes of uncertainty stand out with the NH_3 line spectroscopy being the biggest factor, showing errors of up to 40% in the profile example. The second factor is the signal-to-noise ratio of both instruments which depends on the VMR: under large NH_3 concentrations, the FTIR uncertainty in the signal is in the range of 10%; for measurements with small NH_3 concentrations this greatly increases. Future work should focus on improvements to the NH_3 line spectroscopy to reduce the uncertainty coming from this error source. Furthermore an increased effort is needed to acquire coincident measurements with the FTIR instruments during satellite overpasses as a dedicated validation effort will greatly enhance the number of available observations. Furthermore, a third type of observations measuring the vertical distribution of NH_3 could be used to compare with both the FTIR and CrIS retrievals and further constrain the differences. These observations could be provided by an airborne instrument flying spirals around an FTIR site during a satellite overpass.

5. Data availability

FTIR-NH_3 data (Dammers et al., 2015) can be made available on request (M. Palm, Institut für Umweltphysik, University of Bremen, Bremen, Germany). The CrIS-FRP-NH_3 science grade (non-operational) data products used in this study can be made available on request (M. W. Shephard, Environment and Climate Change Canada, Toronto, Ontario, Canada).The IASI-NH_3 product is freely available at http://www.pole-ether.fr/etherTypo/index.php?id=1700&L=1 (Van Damme et al., 2015a).

~~6.~~

Formatted: Normal, No bullets or numbering

Appendix A.

Formatted: Font: Bold

Formatted: Normal, No bullets or numbering

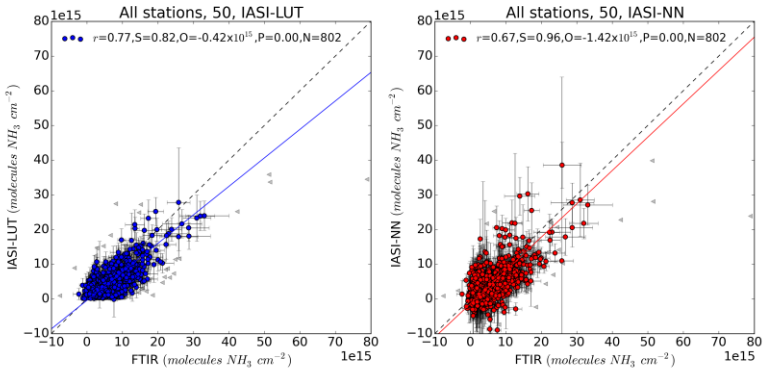

Figure A1. Correlation between the FTIR and the IASI-LUT (left, blue) and IASI-NN (right, red) total columns using the coincident data from all measurement sites. The horizontal and vertical bars show the total estimated error on each FTIR and CrIS observation. A three sigma outlier filter was applied to the IASI-LUT dataset and the same observations were removed from the IASI-NN set. Contrary to the earlier study by Dammers et al., (2016a) no thermal contrast filter was applied to the dataset.

Formatted: Font: Not Bold, English (United Kingdom), Check spelling and grammar

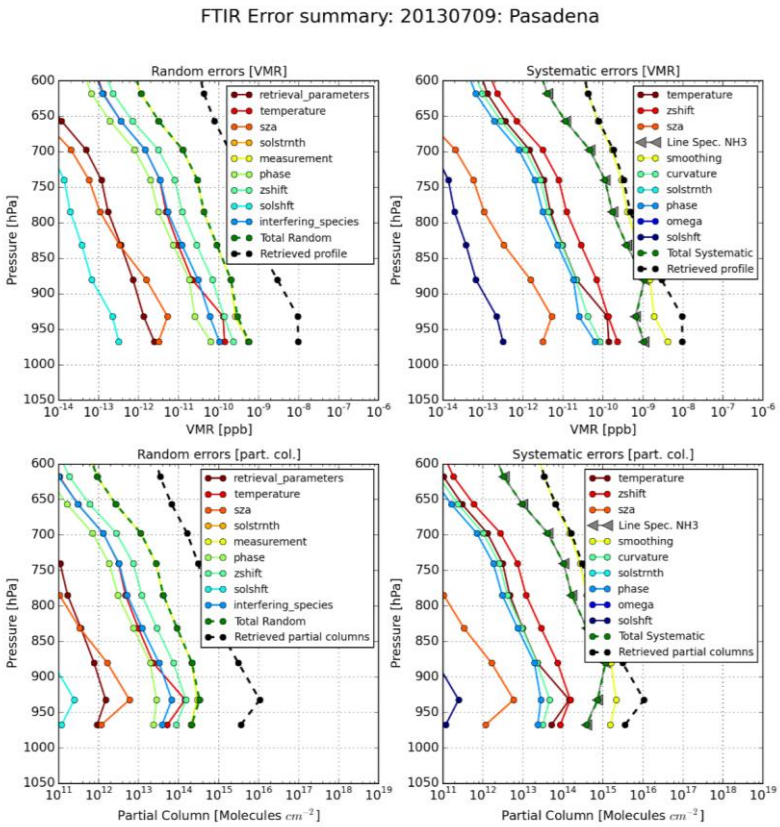

7.

Figure A1A2. Error profiles for each of the error terms. Top The left panels show the random Random errors, bottom the right panels the systematic Systematic errors. Left The top two panels show the error in VMR. Right The bottom panels show the errors in partial column layers [molecules cm^{-2}]. (See Figure A.23 for the same figure but with the errors relative to the final VMR and partial columns per layer)

Formatted: Font: Bold, English (United States)

Formatted: Font: Bold

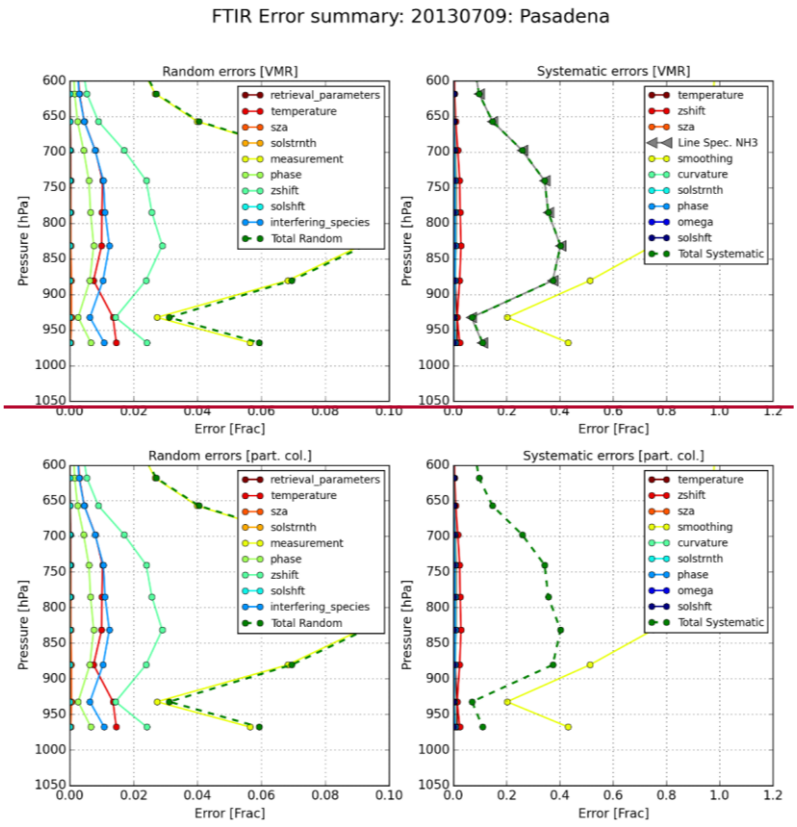
FTIR Error summary: 20130709: Pasadena
Random errors [VMR]
Systematic errors [VMR]
Random errors [part. col.]
Systematic errors [part. col.]
Pressure [hPa]
Error [Frac]
retrieval_parameters
temperature
sza
solstrnth
measurement
phase
zshift
solshft
interfering_species
Total Random
zshift
Line Spec. NH3
smoothing
curvature
omega
Total Systematic

602

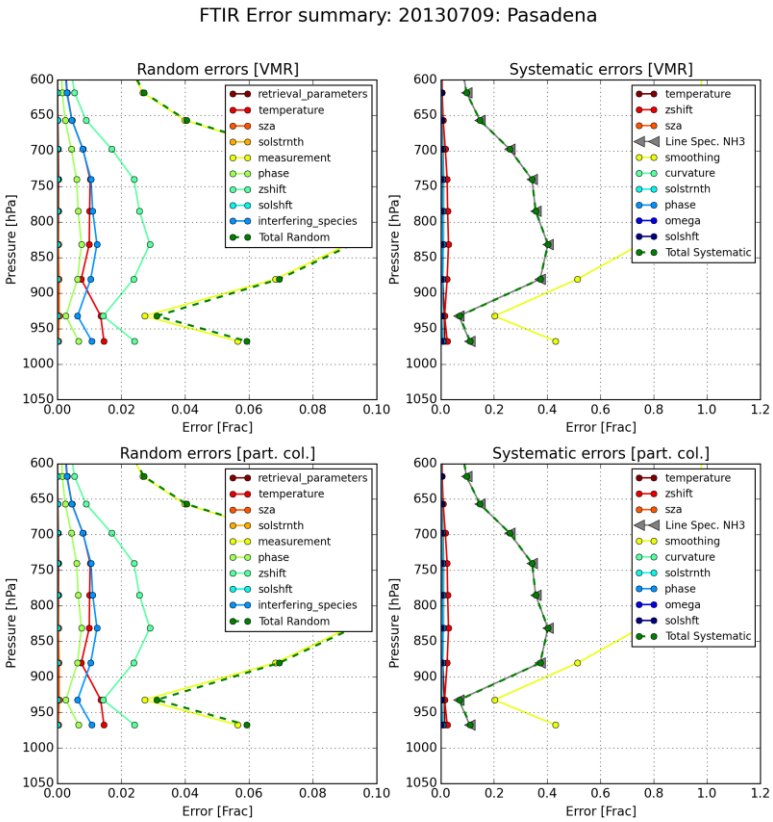

603

604 **Figure ~~A2~~A3.** Relative error profiles for each of the error terms. ~~Top~~ The left panels show the Random errors,
605 ~~bottom~~ right panels the Systematic errors. ~~Left~~ All four panels show the error in a fraction of the original unit
606 used in Figure A2~~two panels show the error in VMR. Right panels show the errors in partial column layers~~
607 ~~[molecules cm^{-2}]~~. (See Figure A~~1~~2 for the same figure but with the absolute errors)

608

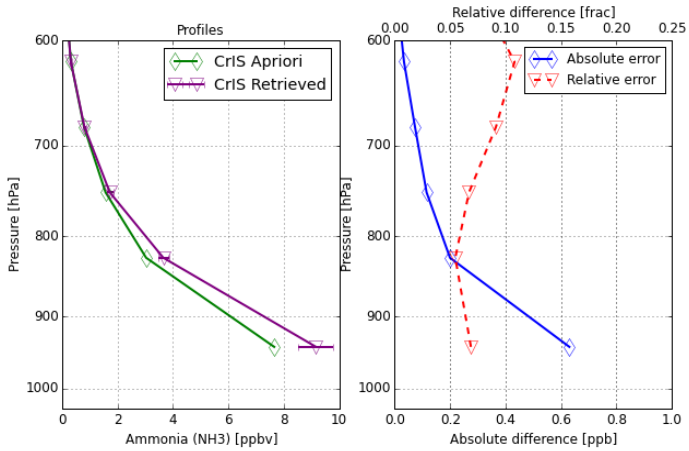

Figure A43. CrIS-NH_3 relative and absolute error profile. The left plot shows the retrieved and a-priori profiles similar to the profiles shown in Figure 5c. The right panel shows the measurement error on the CrIS retrieved profile, with the blue line the absolute value and red line the value relative to the retrieved profile.

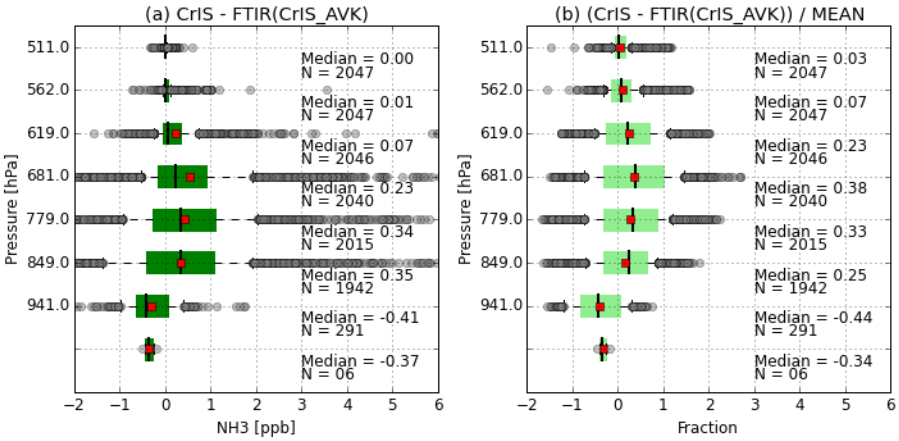

Fig A54. Profile comparison for all stations combined. Observations are combined following pressure "bins", i.e. the midpoints of the CrIS pressure grid. Panel (a) shows the absolute difference [VMR] between profiles (f) and (a). Panel (b) shows the relative difference [Fraction] between the profiles in (Fig 6e) and (Fig 6b). Each of the boxes edges are the 25th and 75th percentiles, the black lines in each box is the median, the red square ~~diamond~~ is the mean, the whiskers are the 10th and 90th percentiles, and the grey circles are the outlier values outside the whiskers.

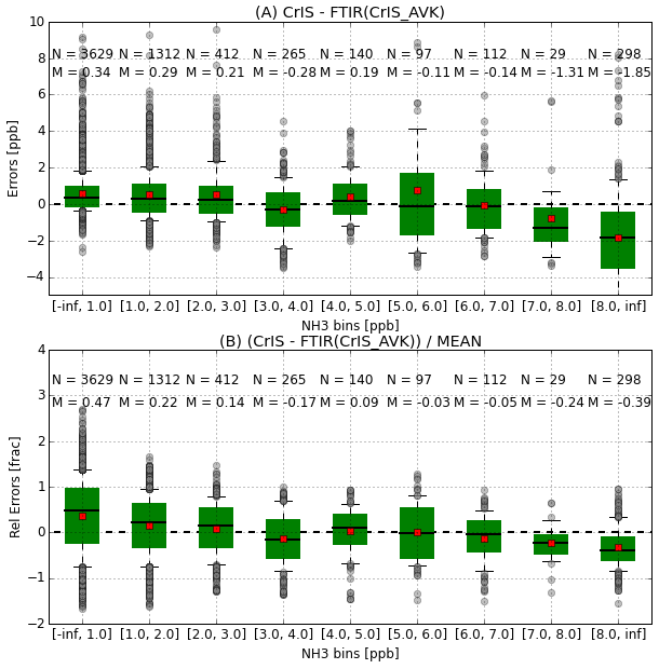

Fig A~~5~~6. Summary of the absolute and relative actual error ~~Summary of the errors~~ as a function of the VMR of NH_3 in the individual FTIR layers. The box edges are the 25th and 75th percentiles, the black line in the box is the median, the red square ~~diamond~~ is the mean, the whiskers are the 10th and 90th percentiles, and the grey circles are the outlier values outside the whiskers. Only observations with a pressure greater than 650 hPa are used. The top panel shows the absolute difference for each VMR bin, the bottom panel shows the relative difference for each VMR bin.

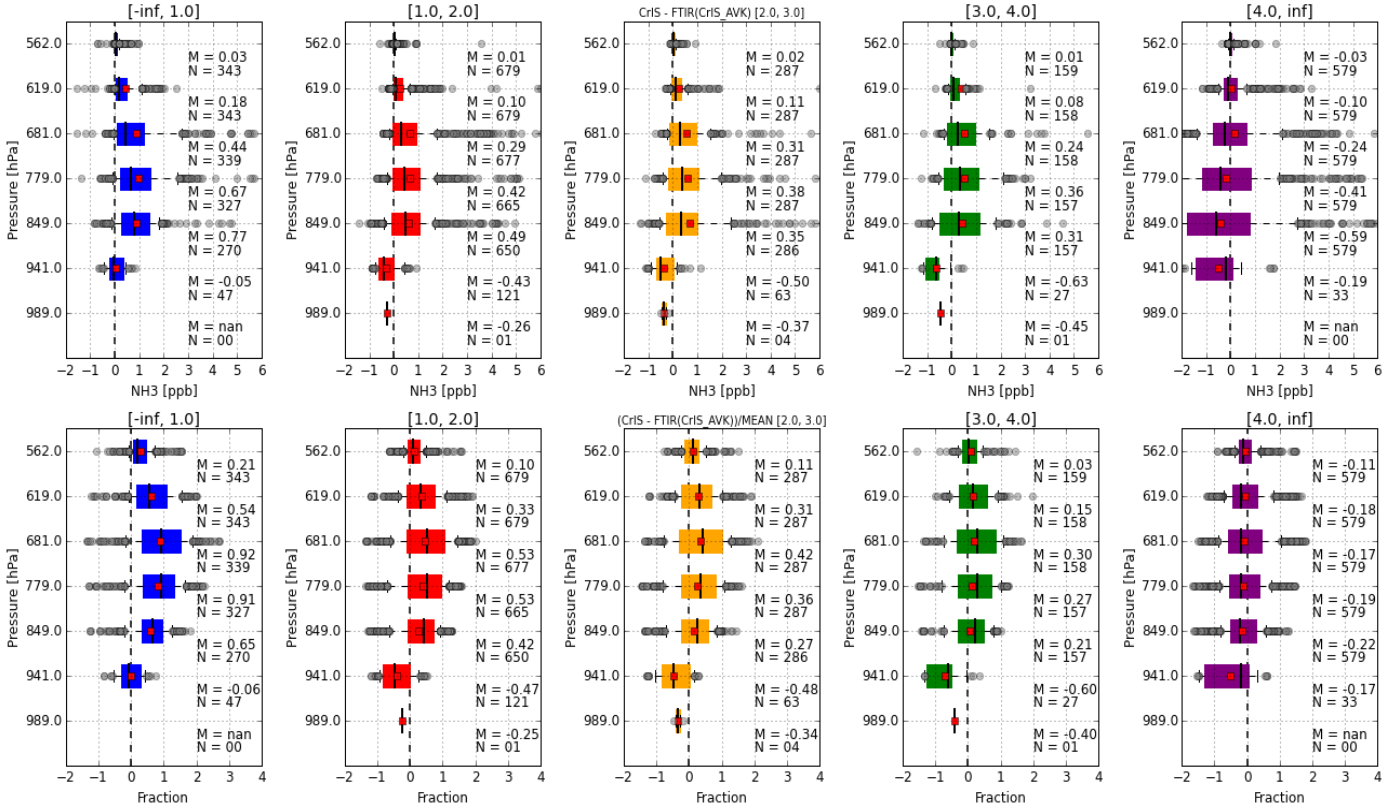

Fig A~~6~~7. Summary of actual errors as a function of VMR. The maximum VMR of each FTIR profiles is used for the classification. Absolute (Top row) and relative profile differences (bottom row) following the FTIR (CrIS AVK applied) and CrIS profiles. Observations are following pressure layers, i.e. the midpoints of the CrIS pressure grid. The box edges are the 25th and 75th percentiles, the black line in the box is the median, the red square ~~diamond~~ is the mean, the whiskers are the 10th and 90th percentiles, and the grey circles are the outlier values outside the whiskers.

Acknowledgements

This work is part of the research programme GO/12-36, which is financed by the Netherlands Organisation for Scientific Research (NWO). This work was also funded at AER through a NASA funded (contract: NNH15CM65C). We would like to acknowledge the University of Wisconsin-Madison Space Science and Engineering Center Atmosphere SIPS team sponsored under NASA contract NNG15HZ38C for providing us with the CrIS level 1 and 2 input data, in particular Liam Gumley. We would also like to thank Andre Wehe (AER) ~~and Jacob Siemons (ECCC)~~ for developing the CrIS download and extraction software. The IASI-LUT and IASI-NN were obtained from the atmospheric spectroscopy group at ULB (Spectroscopie de l'Atmosphère, Service de Chimie Quantique et Photophysique, Université Libre de Bruxelles, Brussels, Belgium) and we would like to thank Simon Whitburn, Martin Van Damme, Lieven Clarisse and Pierre Francois Coheur for their help and contributions. Part of this work was performed at the Jet Propulsion Laboratory, California Institute of Technology, under contract with NASA. The University of Toronto FTIR retrievals were supported by the CAFTON project, funded by the Canadian Space Agency's FAST programme. Measurements were made at the University of Toronto Atmospheric Observatory (TAO), which has been supported by CFCAS, ABB Bomem, CFI, CSA, EC, NSERC, ORDCF, PREA, and the University of Toronto. Funding support in Mexico City was provided by UNAM-DGAPA grants IN107417 & IN112216. A. Bezanilla and B. Herrera participated in the FTIR measurements and M.A. Robles, W. Gutiérrez and M. García are thanked for technical support. We would also like to thank Roy Wichink Kruit and Margreet van Marle for the numerous discussions and valuable input on the subject.

References

Adams, P.J., Seinfeld, J.H., Koch, D., Mickley, L., Jacob, D. (2001), General circulation model assessment of direct radiative forcing by the sulfate-nitrate-ammonium-water inorganic aerosol system, Journal of Geophysical Research Atmospheres, 106 (1), pp. 1097-1111.

Alvarado, M. J., Payne, V. H., Mlawer, E. J., Uymin, G., Shephard, M. W., Cady-Pereira, K. E., Delamere, J. S., and Moncet, J.-L.: Performance of the Line-By-Line Radiative Transfer Model (LBLRTM) for temperature, water vapor, and trace gas retrievals: recent updates evaluated with IASI case studies, Atmos. Chem. Phys., 13, 6687–6711, doi:10.5194/acp-13-6687-2013, 2013

Beer, R., Shephard, M. W., Kulawik, S. S., Clough, S. a., Eldering, A., Bowman, K. W., Sander, S. P., Fisher, B. M., Payne, V. H., Luo, M., Osterman, G. B. and Worden, J. R.: First satellite observations of lower tropospheric ammonia and methanol, Geophys. Res. Lett., 35(9), 1–5, doi:10.1029/2008GL033642, 2008.

Bevington, P. R. and Robinson D. K. (1992) "Data Reduction and Error Analysis for the Physical Sciences, 2nd Ed." pp: 104, and 108-109, McGraw-Hill, New York.

Bezanilla A., Krueger A., Stremme W. and Grutter M. Solar absorption infrared spectroscopic measurements over Mexico City: Methane enhancements. Atmósfera 27(2), 173-183 (2014).

Bobbink, R, Hicks K, Galloway J, Spranger T, Alkemade R, Ashmore M, Bustamante M, Cinderby S, Davidson E, Dentener F, Emmett B, Erisman JW, Fenn M, Gilliam F, Nordin A, Pardo L, De Vries W. Global assessment of nitrogen deposition effects on terrestrial plant diversity: a synthesis, Ecological Applications, 20 (2010), pp. 30–59.

von Bobrutzki, K., Braban, C. F., Famulari, D., Jones, S. K., Blackall, T., Smith, T. E. L., Blom, M., Coe, H., Gallagher, M., Ghalaieny, M., McGillen, M. R., Percival, C. J., Whitehead, J. D., Ellis, R., Murphy, J., Mohacsi,

A., Pogany, A., Junninen, H., Rantanen, S., Sutton, M. A., and Nemitz, E.: Field inter-comparison of eleven atmospheric ammonia measurement techniques, Atmos. Meas. Tech., 3, 91-112, doi:10.5194/amt-3-91-2010, 2010.

Brown, L. R., M. R. Gunson, R. A. Toth, F. W. Irion, C. P. Rinsland, and A. Goldman. "1995 atmospheric trace molecule spectroscopy (ATMOS) linelist."Applied optics 35, no. 16 (1996): 2828-2848.

Calisesi, Y., V. T. Soebijanta, and R. van Oss (2005), Regridding of remote soundings: Formulation and application to ozone profile comparison, J. Geophys. Res., 110, D23306, doi:10.1029/2005JD006122.

Chang, L., Palo, S., Hagan, M., Richter, J., Garcia, R., Riggin, D. and Fritts, D.: Structure of the migrating diurnal tide in the Whole Atmosphere Community Climate Model (WACCM), Advances in Space Research, 41(9), 1398–1407, doi:10.1016/j.asr.2007.03.035, 2008.

Clarisse, Lieven, Cathy Clerbaux, Frank Dentener, Daniel Hurtmans, and Pierre-François Coheur. "Global ammonia distribution derived from infrared satellite observations." Nature Geoscience 2, no. 7 (2009): 479-483.

Clarisse, L., Shephard, M. W., Dentener, F., Hurtmans, D., Cady-Pereira, K., Karagulian, F., Van Damme, M., Clerbaux, C. and Coheur, P.-F.: Satellite monitoring of ammonia: A case study of the San Joaquin Valley, J. Geophys. Res., 115(D13), 1–15, doi:10.1029/2009JD013291, 2010.

Clough, S. A., Shephard, M. W., Mlawer, E. J., Delamere, J. S., Iacono, M. J., Cady-Pereira, K., Boukabara, S., and Brown, P. D.: Atmospheric radiative transfer modeling: a summary of the AER codes, J. Quant. Spectrosc. Radiat. T., 91, 233–244, 2005.

Coheur, P.-F., Clarisse, L., Turquety, S., Hurtmans, D., and Clerbaux, C.: IASI measurements of reactive trace species in biomass burning plumes, Atmos. Chem. Phys., 9, 5655-5667, doi:10.5194/acp-9-5655-2009, 2009.

Dammers, E., Vigouroux, C., Palm, M., Mahieu, E., Warneke, T., Smale, D., Langerock, B., Franco, B., Van Damme, M., Schaap, M., Notholt, J., and Erisman, J. W.: Retrieval of ammonia from ground-based FTIR solar spectra, Atmos. Chem. Phys., 15, 12789-12803, doi:10.5194/acp-15-12789-2015, 2015.

Dammers, E., Palm, M., Van Damme, M., Vigouroux, C., Smale, D., Conway, S., Toon, G. C., Jones, N., Nussbaumer, E., Warneke, T., Petri, C., Clarisse, L., Clerbaux, C., Hermans, C., Lutsch, E., Strong, K., Hannigan, J. W., Nakajima, H., Morino, I., Herrera, B., Stremme, W., Grutter, M., Schaap, M., Wichink Kruit, R. J., Notholt, J., Coheur, P.-F., and Erisman, J. W.: An evaluation of IASI-NH3 with ground-based Fourier transform infrared spectroscopy measurements, Atmos. Chem. Phys., 16, 10351-10368, doi:10.5194/acp-16-10351-2016, 2016a.

Dammers, E., Palm, M., Van Damme, M., Shephard, M., Cady-Pereira, K., Capps, S., Clarisse, L., Coheur, P. and Erisman, J. W.: Validation of NH3 satellite observations by ground-based FTIR measurements, in EGU General Assembly Conference Abstracts, vol. 18, p. 1657., 2016b.

Dentener, F., Drevet, J., Lamarque, J. F., Bey, I., Eickhout, B., Fiore, A. M., Hauglustaine, D., Horowitz, L. W., Krol, M., Kulshrestha, U. C., Lawrence, M., Galy-Lacaux, C., Rast, S., Shindell, D., Stevenson, D., Van Noije, T., Atherton, C., Bell, N., Bergman, D., Butler, T., Cofala, J., Collins, B., Doherty, R., Ellingsen, K., Galloway, J., Gauss, M., Montanaro, V., Müller, J. F., Pitari, G., Rodriguez, J., Sanderson, M., Solmon, F., Strahan, S., Schultz, M., Sudo, K., Szopa, S. and Wild, O.: Nitrogen and sulfur deposition on regional and global scales: A multimodel evaluation, Global Biogeochem. Cycles, 20(4), doi:10.1029/2005GB002672, 2006.

Erisman, J. W., Bleeker, a., Galloway, J. and Sutton, M. S.: Reduced nitrogen in ecology and the environment, Environ. Pollut., 150(1), 140–149, doi:10.1016/j.envpol.2007.06.033, 2007.

Erisman, J.W., Sutton, M.A., Galloway, J., Klimont, Z. and Winiwarter, W., 2008. How a century of ammonia synthesis changed the world. Nature Geoscience, 1(10), pp.636-639.

Erisman, J. W., Galloway, J., Seitzinger, S., Bleeker, A. and Butterbach-Bahl, K.: Reactive nitrogen in the environment and its effect on climate change, Curr. Opin. Environ. Sustain., 3(5), 281–290, doi:10.1016/j.cosust.2011.08.012, 2011.

Farr, T. G., Rosen, P. a., Caro, E. and Crippen, R.: The Shuttle Radar Topography Mission, Rev. …, (2005), 1–33, doi:10.1029/2005RG000183.1.INTRODUCTION, 2007.

Fowler, D., Coyle, M., Skiba, U., Sutton, M. A., Cape, J. N., Reis, S., Sheppard, L. J., Jenkins, A., Grizzetti, B., Galloway, J. N., Vitousek, P., Leach, A., Bouwman, A. F., Butterbach-Bahl, K., Dentener, F., Stevenson, D., Amann, M. and Voss, M.: The global nitrogen cycle in the twenty-first century, Philos. Trans. R. Soc. London B Biol. Sci., 368(1621) [online] Available from: http://rstb.royalsocietypublishing.org/content/368/1621/20130164.abstract, 2013.

Hase, F., Hannigan, J. W., Coffey, M. T., Goldman, a., Höpfner, M., Jones, N. B., Rinsland, C. P. and Wood, S. W.: Intercomparison of retrieval codes used for the analysis of high-resolution, ground-based FTIR measurements, J. Quant. Spectrosc. Radiat. Transf., 87(1), 25–52, doi:10.1016/j.jqsrt.2003.12.008, 2004.

Hase, F., Demoulin, P., Sauval, A. J., Toon, G. C., Bernath, P. F., Goldman, A., Hannigan, J. W., Rinsland, C. P.: An empirical line-by-line model for the infrared solar transmittance spectrum from 700 to 5000 cm(-1), J. Quant. Spectrosc. Ra., 102, 450–463, doi:10.1016/j.jqsrt.2006.02.026, 2006.

Heald, C. L., Collett Jr., J. L., Lee, T., Benedict, K. B., Schwandner, F. M., Li, Y., Clarisse, L., Hurtmans, D. R., Van Damme, M., Clerbaux, C., Coheur, P.-F., Philip, S., Martin, R. V., and Pye, H. O. T.: Atmospheric ammonia and particulate inorganic nitrogen over the United States, Atmos. Chem. Phys., 12, 10295-10312, doi:10.5194/acp-12-10295-2012, 2012

Holland, E. a., Dentener, F. J., Braswell, B. H. and Sulzman, J. M.: Contemporary and pre-industrial global reactive nitrogen budgets, Biogeochemistry, 46(1-3), 7–43, doi:10.1007/BF01007572, 1999.

Leen, J. B., Yu, X. Y., Gupta, M., Baer, D. S., Hubbe, J. M., Kluzek, C. D., Tomlinson, J. M. and Hubbell, M. R.: Fast in situ airborne measurement of ammonia using a mid-infrared off-axis ICOS spectrometer, Environ. Sci. Technol., 47(18), 10446–10453, doi:10.1021/es401134u, 2013.

Lonsdale, C. R., Hegarty, J. D., Cady-Pereira, K., Alvarado, M. J., Henze, D. K., Turner, M. D., Capps, S. L., Nowak, J. B., Neuman, J. A., Middlebrook, A. M., Bahreini, R., Murphy, J. G., Markovic, M., VandenBoer, T. C., Russell, L. M., and Scarino, A. J.: Modeling the Diurnal Variability of Agricultural Ammonia in Bakersfield, California during CalNex, Atmos. Chem. Phys. Discuss., doi:10.5194/acp-2016-44, in review, 2016

Lutsch, E., Dammers, E., Conway, S. and Strong, K., 2016. Long-range transport of NH_3, CO, HCN, and C_2H_6 from the 2014 Canadian Wildfires. Geophysical Research Letters, 43(15), pp.8286-8297, doi:10.1002/2016GL070114, 2016.

Miller, D. J., Sun, K., Tao, L., Khan, M. A., and Zondlo, M. A.: Open-path, quantum cascade-laser-based sensor for high-resolution atmospheric ammonia measurements, Atmos. Meas. Tech., 7, 81-93, doi:10.5194/amt-7-81-2014, 2014

Moncet, J.-L, X. Liu, H. Snell, J. Eluszkiewicz, Y. He, T. Kennelly, R. Lynch, S. Boukabara, A. Lipton, H. Rieu-Isaacs, G. Uymin, and S. Zaccheo : Algorithm Theoretical Basis Document for the Cross-track Infrared Sounder Environmental Data Records, AER Document Number: P1187-TR-I-08, Version 4.2, available at: http://www.star.nesdis.noaa.gov/jpss/documents/ATBD/D0001-M01-S01-007_JPSS_ATBD_CrIMSS_B.pdf, (last access date: 24 October 2015), 2005.

Moncet, J.-L, Uymin G., Lipton A. E., and Snell H. E.: Infrared radiance modeling by optimal spectral sampling. J. Atmos. Sci., 65, 3917-3934, 2008.

Morgenstern, O., Zeng, G., Wood, S. W., Robinson, J., Smale, D., Paton-Walsh, C., Jones, N. B., and Griffith, D. W. T.: Long-range correlations in Fourier transform infrared, satellite, and modeled CO in the Southern Hemisphere, J. Geophys. Res., 117, D11301 doi:10.1029/2012JD017639, 2012.

Myhre, G., Shindell, D., Bréon, F.-M., Collins, W., Fuglestvedt, J., Huang, J., Koch, D., Lamarque, J.-F., Lee, D., Mendoza, B., Nakajima, T., Robock, A., Stephens, G., Takemura, T., and Zhang, H.: Anthropogenic and Natural Radiative Forcing, in: Climate Change 2013: The Physical Science Basis. Contribution of Working Group I to the Fifth Assessment Report of the Intergovernmental Panel on Climate Change, edited by: Stocker,

T. F., Qin, D., Plattner, G.-K., Tignor, M., Allen, S. K., Boschung, J., Nauels, A., Xia, Y., Bex, V., and Midgley, P. M., Cambridge University Press, Cambridge, United Kingdom and New York, NY, USA, 2013

Nowak, J. B., Neuman, J. A., Kozai, K., Huey, L. G., Tanner, D. J., Holloway, J. S., Ryerson, T. B., Frost, G. J., McKeen, S. A., and Fehsenfeld, F. C.: A chemical ionization mass spectrometry technique for airborne measurements of ammonia, J. Geophys. Res.-Atmos., 112, D10S02, doi:10.1029/2006JD007589, 2007.

Nowak, J. B., Neuman, J. A., Bahreini, R., Brock, C. A., Middlebrook, A. M., Wollny, A. G., Holloway, J. S., Peischl, J., Ryerson, T. B., and Fehsenfeld, F. C.: Airborne observations of ammonia and ammonium nitrate formation over Houston, Texas, J. Geophys. Res.-Atmos., 115, D22 304, doi:10.1029/ 2010JD014195, 2010.

Nowak, J. B., Neuman, J. A., Bahreini, R., Middlebrook, A. M., Holloway, J. S., McKeen, S. A., Parrish, D. D., Ryerson, T. B. and Trainer, M.: Ammonia sources in the California South Coast Air Basin and their impact on ammonium nitrate formation, Geophys. Res. Lett., 39(7), 2012.

Oren, R., Ellsworth, D.S., Johnsen, K.H., Phillips, N., Ewers, B.E., Maier, C., Schäfer, K.V., McCarthy, H., Hendrey, G., McNulty, S.G. and Katul, G.G., 2001. Soil fertility limits carbon sequestration by forest ecosystems in a CO2-enriched atmosphere. Nature, 411(6836), pp.469-472.

Pope III, C. A., Burnett, R. T., Thun, M. J., Calle, E. E., Krewski, D., Ito, K. and Thurston, G. D.: Lung cancer, cardiopulmonary mortality, and long-term exposure to fine particulate air pollution, Jama, 287(9), 1132–1141, 2002.

Pope, III, C. A., Ezzati, M., and Dockery, D. W.: Fine-Particulate Air Pollution and Life Expectancy in the United States, N. Engl. J. Med., 360, 376–386, doi:{10.1056/NEJMsa0805646}, 2009.

Pougatchev, N. S., Connor, B. J., & Rinsland, C. P. (1995). Infrared measurements of the ozone vertical distribution above Kitt Peak. Journal of Geophysical Research: Atmospheres (1984–2012), 100(D8), 16689-16697.

Puchalski, M. A., M. E. Sather, J. T. Walker, C. M. Lehmann, D. A. Gay, J. Mathew, and W. P. Robarge (2011), Passive ammonia monitoring in the United States: Comparing three different sampling devices, J. Environ. Monit., 13(11), 3156–3167, doi:10.1039/c1em10553a.

Reis, S., Pinder, R. W., Zhang, M., Lijie, G., and Sutton, M. A.: Reactive nitrogen in atmospheric emission inventories, Atmos. Chem. Phys., 9, 7657-7677, doi:10.5194/acp-9-7657-2009, 2009

Rockstrom, J., Steffen, W., Noone, K., Persson, A., Chapin, F. S., Lambin, E. F., Lenton, T. M., Scheffer, M., Folke, C., Schellnhuber, H. J., Nykvist, B., de Wit, C. A., Hughes, T., van der Leeuw, S., Rodhe, H., Sorlin, S., Snyder, P. K., Costanza, R., Svedin, U., Falkenmark, M., Karlberg, L., Corell, R. W., Fabry, V. J., Hansen, J., Walker, B., Liverman, D., Richardson, K., Crutzen, P. and Foley, J. A.: A safe operating space for humanity, Nature, 461(7263), 472–475 [online] Available from: http://dx.doi.org/10.1038/461472a, 2009.

Rodgers, C. D.: Inverse methods for atmospheric Sounding: Theory and Practice, World Sci., Hackensack, NJ, 2000.

Rodgers, C. D. and Connor, B. J.: Intercomparison of remote sounding instruments, J. Geophys. Res. Atmos., 108(D3), n/a–n/a, doi:10.1029/2002JD002299, 2003.

Rodhe, Henning, Frank Dentener, and Michael Schulz. "The global distribution of acidifying wet deposition." Environmental Science & Technology 36.20 (2002): 4382-4388.

Rothman, L. S., Gordon, I. E., Babikov, Y., Barbe, a., Chris Benner, D., Bernath, P. F., Birk, M., Bizzocchi, L., Boudon, V., Brown, L. R., Campargue, a., Chance, K., Cohen, E. a., Coudert, L. H., Devi, V. M., Drouin, B. J., Fayt, a., Flaud, J. M., Gamache, R. R., Harrison, J. J., Hartmann, J. M., Hill, C., Hodges, J. T., Jacquemart, D., Jolly, a., Lamouroux, J., Le Roy, R. J., Li, G., Long, D. a., Lyulin, O. M., Mackie, C. J., Massie, S. T., Mikhailenko, S., Müller, H. S. P., Naumenko, O. V., Nikitin, a. V., Orphal, J., Perevalov, V., Perrin, a., Polovtseva, E. R., Richard, C., Smith, M. a H., Starikova, E., Sung, K., Tashkun, S., Tennyson, J., Toon, G. C., Tyuterev, V. G. and Wagner, G.: The HITRAN2012 molecular spectroscopic database, J. Quant. Spectrosc. Radiat. Transf., 130, 4–50, doi:10.1016/j.jqsrt.2013.07.002, 2013.

Schaap, M., van Loon, M., ten Brink, H. M., Dentener, F. J., and Builtjes, P. J. H.: Secondary inorganic aerosol simulations for Europe with special attention to nitrate, Atmos. Chem. Phys., 4, 857-874, doi:10.5194/acp-4-857-2004, 2004.

Schiferl, L. D., Heald, C. L., Nowak, J. B., Holloway, J. S., Neuman, J. A., Bahreini, R., Pollack, I. B., Ryerson, T. B., Wiedinmyer, C., and Murphy, J. G.: An investigation of ammonia and inorganic particulate matter in California during the CalNex campaign, J. Geophys. Res.-Atmos., 119, 1883–1902, doi:10.1002/2013JD020765, 2014.

Schiferl, L. D., Heald, C. L., Van Damme, M., Clarisse, L., Clerbaux, C., Coheur, P.-F., Nowak, J. B., Neuman, J. A., Herndon, S. C., Roscioli, J. R., and Eilerman, S. J.: Interannual variability of ammonia concentrations over the United States: sources and implications, Atmos. Chem. Phys., 16, 12305-12328, doi:10.5194/acp-16-12305-2016, 2016

Seinfeld, J. H. and Pandis, S. N.: Atmospheric Chemistry and Physics, John Wiley, Hoboken, NJ, 1988.

Shephard, M.W., Clough, S. A., Payne, V. H., Smith,W. L., Kireev, S., and Cady-Pereira, K. E.: Performance of the line-by-line radiative transfer model (LBLRTM) for temperature and species retrievals: IASI case studies from JAIVEx, Atmos. Chem. Phys., 9, 7397–7417, doi:10.5194/acp-9-7397-2009, 2009.

Shephard, M. W., Cady-Pereira, K. E., Luo, M., Henze, D. K., Pinder, R. W., Walker, J. T., Rinsland, C. P., Bash, J. O., Zhu, L., Payne, V. H., and Clarisse, L.: TES ammonia retrieval strategy and global observations of the spatial and seasonal variability of ammonia, Atmos. Chem. Phys., 11, 10743-10763, doi:10.5194/acp-11-10743-2011, 2011

Shephard, M. W. and Cady-Pereira, K. E.: Cross-track Infrared Sounder (CrIS) satellite observations of tropospheric ammonia, Atmos. Meas. Techn., 8, 1323–1336, doi:10.5194/amt-8-1323-2015, http://www.atmos-meas-tech.net/8/1323/2015/, 2015.

Shephard, M. W., McLinden, C. A., Cady-Pereira, K. E., Luo, M., Moussa, S. G., Leithead, A., Liggio, J., Staebler, R. M., Akingunola, A., Makar, P., Lehr, P., Zhang, J., Henze, D. K., Millet, D. B., Bash, J. O., Zhu, L., Wells, K. C., Capps, S. L., Chaliyakunnel, S., Gordon, M., Hayden, K., Brook, J. R., Wolde, M., and Li, S.-M.: Tropospheric Emission Spectrometer (TES) satellite observations of ammonia, methanol, formic acid, and carbon monoxide over the Canadian oil sands: validation and model evaluation, Atmos. Meas. Tech., 8, 5189-5211, doi:10.5194/amt-8-5189-2015, 2015.

Sun, K., Cady-Pereira, K., Miller, D. J. , Tao, L., Zondlo, M.A. , Nowak, J. B., Neuman, J. A., Mikoviny, T., Müller, M. ,Wisthaler, A., Scarino, A. J., and Hostetler, C. A.: Validation of TES ammonia observations at the single pixel scale in theSan Joaquin Valley during DISCOVER-AQ, J. Geophys. Res.-Atmos., 120, 5140–5154, doi:10.1002/2014JD022846, 2015.

Sutton, M. a, Reis, S., Riddick, S. N., Dragosits, U., Nemitz, E., Theobald, M. R., Tang, Y. S., Braban, C. F., Vieno, M., Dore, A. J., Mitchell, R. F., Wanless, S., Daunt, F., Fowler, D., Blackall, T. D., Milford, C., Flechard, C. R., Loubet, B., Massad, R., Cellier, P., Personne, E., Coheur, P. F., Clarisse, L., Van Damme, M., Ngadi, Y., Clerbaux, C., Skjøth, C. A., Geels, C., Hertel, O., Wichink Kruit, R. J., Pinder, R. W., Bash, J. O., Walker, J. T., Simpson, D., Horváth, L., Misselbrook, T. H., Bleeker, A., Dentener, F. and de Vries, W.: Towards a climate-dependent paradigm of ammonia emission and deposition., Philos. Trans. R. Soc. Lond. B. Biol. Sci., 368(1621), 20130166, doi:10.1098/rstb.2013.0166, 2013.

Tobin, D.: Early Checkout of the Cross-track Infrared Sounder (CrIS) on Suomi-NPP, Through the Atmosphere, Summer 2012, available at: www.ssec.wisc.edu/news/media/2012/07/ttasummer20121.pdf (last access date: 30 January 2017), 2012.

Toon, G. C., Blavier, J.-F., Sen, B., Margitan, J. J., Webster, C. R., Max, R. D., Fahey, D. W., Gao, R., DelNegro, L., Proffitt, M., Elkins, J., Romashkin, P. A., Hurst, D. F., Oltmans, S., Atlas, E., Schauffler, S., Flocke, F., Bui, T. P., Stimpfle, R. M., Bonne, G. P., Voss, P. B., and Cohen, R. C.: Comparison of MkIV balloon and ER-2 aircraft measurements of atmospheric trace gases, J. Geophys. Res., 104, 26 779–26 790, 1999.

Van Damme, M., Clarisse, L., Heald, C. L., Hurtmans, D., Ngadi, Y., Clerbaux, C., Dolman, A. J., Erisman, J. W., and Coheur, P. F.: Global distributions, time series and error characterization of atmospheric ammonia (NH3) from IASI satellite observations, Atmos. Chem. Phys., 14, 2905-2922, doi:10.5194/acp-14-2905-2014, 2014a.

Van Damme, M., R. J. Wichink Kruit, M. Schaap, L. Clarisse, C. Clerbaux, P.-F. Coheur, E. Dammers, A. J. Dolman, and J. W. Erisman , Evaluating 4 years of atmospheric ammonia (NH3) over Europe using IASI satellite observations and LOTOS-EUROS model results, J. Geophys. Res. Atmos., 119, 9549–9566, doi:10.1002/2014JD021911, 2014b.

Van Damme, M., J. W. Erisman, L. Clarisse, E. Dammers, S. Whitburn, C. Clerbaux, A. J. Dolman, and P.-F. Coheur (2015a), Worldwide spatiotemporal atmospheric ammonia (NH3) columns variability revealed by satellite, Geophys. Res. Lett., 42, doi:10.1002/2015GL065496.

Van Damme, M., Clarisse, L., Dammers, E., Liu, X., Nowak, J. B., Clerbaux, C., Flechard, C. R., Galy-Lacaux, C., Xu, W., Neuman, J. a., Tang, Y. S., Sutton, M. a., Erisman, J. W. and Coheur, P. F.: Towards validation of ammonia (NH3) measurements from the IASI satellite, Atmos. Meas. Tech., 8(3), 1575–1591, doi:10.5194/amt-8-1575-2015, 2015b.

Velazco, V., Wood, S. W., Sinnhuber, M., Kramer, I., Jones, N. B., Kasai, Y., Notholt, J., Warneke, T., Blumenstock, T., Hase, F., Murcray, F. J., and Schrems, O.: Annual variation of strato-mesospheric carbon monoxide measured by ground-based Fourier transform infrared spectrometry, Atmos. Chem. Phys., 7, 1305-1312, doi:10.5194/acp-7-1305-2007, 2007.

Warner, J. X., Wei, Z., Strow, L. L., Dickerson, R. R., and Nowak, J. B.: The global tropospheric ammonia distribution as seen in the 13-year AIRS measurement record, Atmos. Chem. Phys., 16, 5467-5479, doi:10.5194/acp-16-5467-2016, 2016

Whitburn, S., Van Damme, M., Kaiser, J. W., van der Werf, G. R., Turquety, S., Hurtmans, D., Clarisse, L., Clerbaux, C. and Coheur, P.-F.: Ammonia emissions in tropical biomass burning regions: Comparison between satellite-derived emissions and bottom-up fire inventories, Atmos. Environ., 1–13, doi:10.1016/j.atmosenv.2015.03.015, 2015.

Whitburn, S., M. Van Damme, L. Clarisse, S. Bauduin, C. L. Heald, J. Hadji-Lazaro, D. Hurtmans, M. A. Zondlo, C. Clerbaux, and P.-F. Coheur (2016), A flexible and robust neural network IASI-NH3 retrieval algorithm, J. Geophys. Res. Atmos., 121, 6581–6599, doi:10.1002/2016JD024828.

Wiacek, A., Taylor, J. R., Strong, K., Saari, R., Kerzenmacher, T. E., Jones, N. B. and Griffith, D. W. T.: Ground-Based Solar Absorption FTIR Spectroscopy: Characterization of Retrievals and First Results from a Novel Optical Design Instrument at a New NDACC Complementary Station, J. Atmos. Ocean. Technol., 24(3), 432–448, doi:10.1175/JTECH1962.1, 2007.

Worden, J., Kulawik S. S., Shephard M. W., Clough S. A., Worden H., Bowman K., and Goldman A.: Predicted errors of tropospheric emission spectrometer nadir retrievals from spectral window selection, J. Geophys. Res., 109, D09308, doi:10.1029/2004JD004522, 2004.

Zondlo, M., Pan, D., Golston, L., Sun, K. and Tao, L.: Ammonia emissions, transport, and deposition downwind of agricultural areas at local to regional scales, in EGU General Assembly Conference Abstracts, vol. 18, p. 16552., 2016.

Zhu, L., Henze, D. K., Cady-Pereira, K. E., Shephard, M. W., Luo, M., Pinder, R. W., Bash, J. O. and Jeong, G. R.: Constraining U.S. ammonia emissions using TES remote sensing observations and the GEOS-Chem adjoint model, J. Geophys. Res. Atmos., 118(8), 3355–3368, doi:10.1002/jgrd.50166, 2013.